Universität Stuttgart

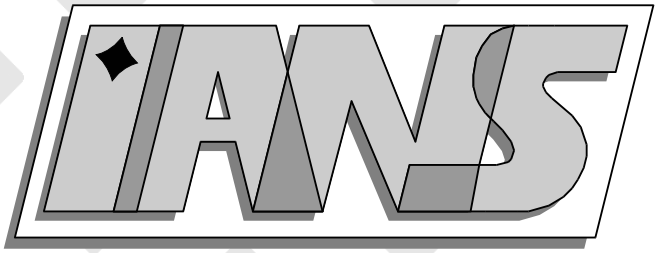

Analytical and numerical treatment of a dynamic crack model

Adriana Lalegname, Anna-Margarete Sändig, Granville Sewell

Berichte aus dem Institut für Angewandte Analysis und Numerische Simulation

preprint 2008/004

Universität Stuttgart

Analytical and numerical treatment of a dynamic crack model

Adriana Lalegname, Anna-Margarete Sändig, Granville Sewell

Berichte aus dem Institut für Angewandte Analysis und Numerische Simulation

preprint 2008/004

Institut für Angewandte Analysis und Numerische Simulation (IANS)
Fakultät Mathematik und Physik
Fachbereich Mathematik
Pfaffenwaldring 57
D-70 569 Stuttgart

E-Mail: ians-preprints@mathematik.uni-stuttgart.de
WWW: http://preprints.ians.uni-stuttgart.de

ISSN **1611-4176**

ANALYTICAL AND NUMERICAL TREATMENT OF A DYNAMIC CRACK MODEL.

A. LALEGNAME[1], A.-M. SÄNDIG[1], AND G. SEWELL[2]

Abstract. We discuss the propagation of a running crack in a bounded linear elastic body under shear waves for a simplified 2D-model. This model is described by two coupled equations in the actual configuration: a two-dimensional scalar wave equation in a cracked, bounded domain and an ordinary differential equation derived from an energy balance law. The unknowns are the displacement fields $u = u(y,t)$ and the one-dimensional crack tip trajectory $h = h(t)$. We assume that the crack grows straight. Based on the paper [22] we derive an improved formula for the ordinary differential equation of motion for the crack tip, where the dynamical stress intensity factor occurs. The numerical simulation is an iterative procedure starting from the wave field at time $t = t_i$. The dynamic stress intensity factor will be extracted at $t = t_i$. Its knowledge allows us to compute the crack-tip motion $h(t_{i+1})$ with corresponding nonuniform crack speed assuming $(t_{i+1} - t_i)$ is small. Now, we start from the cracked configuration at time $t = t_{i+1}$ and repeat the steps. The wave displacements are computed with the FEM-package PDE2D [25] Some numerical examples demonstrate the proposed method.

[1] University of Stuttgart, Institute of Applied Analysis and Numerical Simulation, Pfaffenwaldring 57, 70569 Stuttgart, Germany. lalegname/saendig@mathematik.uni-stuttgart.de

[2] Mathematics Department,University of Texas El Paso, El Paso, Texas 79968, sewell@math.utep.edu

1. Introduction

To analyze the crack-tip behavior theoretically a number of approaches have been derived [4], [12],[14]. However, there are many unsolved problems in dynamic fracture mechanics. In this paper we investigate mathematically the behaviour of a linear elastic body with a crack under the influence of an incident wave. Reducing the three-dimensional wave model for a linear elastic, isotropic and homogeneous body to a two-dimensional one we get an in-plane model for plane elastic waves and an out-of-plane model for shear waves. Here, we investigate the simpler out-of-plane state as a model. The extension of our method to the in-plane state is possible and will be done in the future.

We assume that the 2D solid contains exactly one finite, straight pre-crack σ_0, which may expand in a straight line along the horizontal axis y_1. Starting from a crack with length l, the crack tip position at time t is given by $h = h(t)$. Besides this unknown quantity h the displacement field $u = u(y_1, y_2, t)$ is the unknown solution of the wave equation in the cracked domain. The unknowns h and u are coupled, through a system of an initial-boundary value problem for the wave equation (2.3) and an initial value problem for an ordinary differential equation (1.1) derived from an energy balance law. The latter problem reads: Find $h = h(t)$ such that:

$$\Gamma(h, h') = k^2(t, h, h')c^2\frac{\pi}{4}, \quad h(0) = 0. \tag{1.1}$$

Here $\Gamma(h, h')$ represents the dynamic fracture toughness, a material property measuring the fracture resistance. It can be found only experimentally and is not easy to determine. The constant c is the shear wave speed, $k(t, h, h')$ is the stress intensity factor, which responds instantaneously to a change in crack propagation velocity $h'(t)$ and it includes the effects of loading and geometry.

The mathematical analysis of the full coupled nonlinear problem seems to be difficult and we consider an iterative approach starting from the given pre-crack position. Computing the wave-displacement and the dynamic stress intensity factor $k(t, h, h')$ at a certain time $t = t_i$ we use the solution of the ordinary differential equation (1.1) to pass to the next time step $t = t_{i+1}$ and repeat the procedure. This approach is fundamental for the numerical simulations.

It is essential that we can describe the singular behavior of the displacement field near the running crack tip and compute the coefficient in front of the leading dynamic crack singularity, the stress intensity factor $k(t, h, h')$. We get a decomposition of u into a regular term u_R and a singular one (analogously to [7],[13], [18],[21]):

$$u(y, t) = u_R(y, t) + k(t, h, h')\,\eta(y)\,S_N(y_1 - h(t), y_2) \tag{1.2}$$

with

$$S_N(y_1 - h, y_2, t) = \sqrt{\frac{1}{2\alpha(t)}}\sqrt{\sqrt{(R\cos\vartheta - h)^2 + \alpha^2(t)\,R^2\sin^2\vartheta} - (R\cos\vartheta - h)}. \tag{1.3}$$

Here, (R, ϑ) are the actual running polar coordinates and we assume that

$$\alpha(t)^2 = 1 - \frac{h'(t)^2}{c^2} \geq \gamma_0^2 > 0. \tag{1.4}$$

The mathematical analysis is done distinguishing between the actual configuration (space variables y_1, y_2, noncylindric domain), a reference configuration (space variables x_1, x_2, cylindric domain) and a further configuration (space variables z_1, z_2), where the isotropic Laplacian appears. The passage to the different configurations will be clearly described by the corresponding coordinate transformations. We emphasize, that this allows us to start from a energy balance equation in the actual configuration, to transform it into the reference configuration, to treat the crack singularities there and finally to obtain formula (1.1).

Due to its great importance in dynamic fracture mechanics, the computation of the dynamic stress intensity factor has attracted much attention from engineers [33], [39], [40]. However, we mention that to our knowledge the analytical model proposed here and the numerical simulation of the crack tip motion $h(t)$ and the corresponding nonuniform crack tip speed $h'(t)$, are new.

The paper is organized as follows: In **section 2** we sketch the derivation of the coupled mathematical model following some ideas of the paper [22]. Since an error concerning formula (1.1) is contained in [22] we should improve the corresponding results from [22].
Section 3 deals with numerical simulations. Based on the analytical results from section 2 we present pertinent novel numerical results. To compute both unknowns, the displacement field $u(y,t)$ and the crack tip motion $h(t)$, of the coupled problem and to demonstrate the interaction of the shear wave with the propagation of the crack, an iterative numerical procedure is proposed and implemented using the FEM-package PDE2D [25]. Two different examples for the dynamical propagation of a mode III crack, will be analysed here.
The solution of the wave equation (2.3) has a singular behavior near the crack tip $h = h(t)$ even when f is very smooth. Such singular behavior affects the accuracy of the finite element method throughout the whole domain. The decomposition (1.2) will be used quite often in order to calculate accurate finite element approximations to both the solution and the dynamic stress intensity factor.

2. The mathematical model

Elastic waves are often modeled by the linear Navier-Lamé equation system in a three-dimensional space-domain:

$$\rho u_{tt} - (\mu \Delta u + (\lambda + \mu)\ \mathrm{grad}(\div u)) = \tilde{f} \tag{2.1}$$

where $u(y,t) = u = (u_1, u_2, u_3)^T$ is the displacement field, ρ the mass-density, λ, μ the Lamé coefficients and $\tilde{f}(y,t) = \tilde{f} = (\tilde{f}_1, \tilde{f}_2, \tilde{f}_3)^T$ is the density vector of the volume forces. We study a simpler model for the out-of plane state, that means we assume that $u_1 = u_2 = 0, u_3 = u$ and $\partial_3 u_3 = 0$. Then the system (2.1) reduces to a scalar wave equation

$$u_{tt} - c^2 \Delta u = f, \tag{2.2}$$

where $f = \frac{\tilde{f}_3}{\rho}$, $c^2 = \frac{\mu}{\rho}$. Here $c = \sqrt{\frac{\mu}{\rho}}$ is the speed of the shear waves which is quite large (for steel $c \approx 3200\ [\frac{m}{s}]$ or for glass $c \approx 3300\ [\frac{m}{s}]$).

We will study an initial-boundary value problem for the wave equation (2.2) in the cracked domain $Q = \cup_{t=0}^{T} \Omega_t$, see Fig. 1.

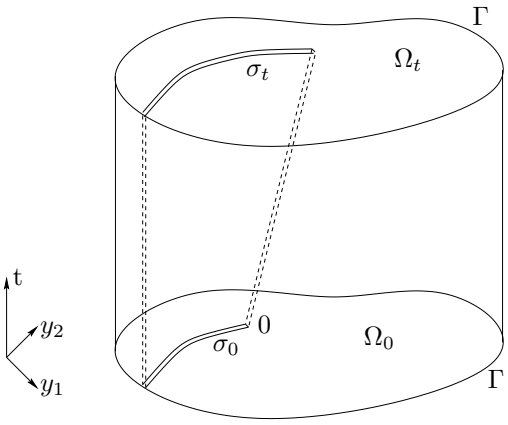

Figure 1: noncylindrical domain Q

Find $u = u(y,t)$ such that

$$\left.\begin{aligned} &\partial_t^2 u - c^2 \Delta u = f \text{ in } Q := \cup_{t=0}^{T} \Omega_t, \\ &c^2 \partial_n u = 0 \text{ on } \cup_{t=0}^{T} \sigma_t, \\ &c^2 \partial_n u = q \text{ on } \Sigma_N := \Gamma_N \times (0,T), \\ &u = 0 \text{ on } \Sigma_D := \Gamma_D \times (0,T), \\ &u(0) = u_0,\ \partial_t u(0) = u_1 \text{ in } \Omega_0, \end{aligned}\right\} \tag{2.3}$$

where $\overline{\Gamma}_D \cup \overline{\Gamma}_N = \Gamma$ and $\Gamma_D \cap \Gamma_N = \emptyset$. On Γ_N, $\partial_n u = \nabla u \cdot n$ means the outward normal derivative while on σ_t it means the normal derivative in one fixed normal direction (therefore $\partial_n u = 0$ on σ_t means that the normal derivative from above and from below are both zero). The domain Ω_0 with the pre-crack σ_0 is the reference domain, whereas the domains Ω_t form a family of actual configurations. We assume, that the motion of Ω_0 to Ω_t is given by a family of mappings

$$y = F_t(x) = x + h(t)\ \theta(x), \quad x \in \Omega_0, \quad y \in \Omega_t, \tag{2.4}$$

Here,

$$\theta(x) = \eta(r) \begin{pmatrix} 1 \\ 0 \end{pmatrix}, \tag{2.5}$$

where $\eta = \eta(r)$ is a smooth cut-off function such that $\eta \equiv 1$ in a neighborhood of the crack tip $\{0\}$ and as usual $r = |x-0| = |x|$ is the distance to the crack tip $\{0\}$. Note that F_t is a diffeomorphism from $\Omega = \Omega_0$ onto Ω_t and

$$\det \nabla F_t = \det(I + h\nabla\theta) \geq D_0 > 0 \quad \text{for } (x,t) \in \bar{\Omega} \times [0,T] \tag{2.6}$$

for some positive constant D_0 independent of x and t, where

$$\nabla\theta = \begin{pmatrix} \partial_1\theta_1 & \partial_2\theta_1 \\ \partial_1\theta_2 & \partial_2\theta_2 \end{pmatrix}$$

is the Jacobian matrix of θ.

The following mathematical difficulty occurs: problem (2.3) is given in a noncylindrical domain Q. To our knowledge there are no existence, uniqueness and regularity results available. Therefore we transform (2.3) by (2.4) to the cylindrical domain $\Omega_0 \times (0,T)$ setting:

$$\begin{aligned} u(y,t) &= u(F_t(x),t) =: v(x,t), \\ f(y,t) &= f(F_t(x),t) =: \hat{f}(x,t) \\ q(y,t) &= q(F_t(x),t) =: \hat{q}(x,t) \end{aligned} \tag{2.7}$$

Lemma 2.1. [22] *The change of variables (2.4) leads to the following transformed problem in the reference configuration Ω_0 :*

$$v_{tt} + \mathcal{A}_0(t)\, v + \mathcal{A}_1(t)\, v + \mathcal{B}(t)\, v_t = \hat{f} \text{ in } \Omega_0 \times (0,T), \tag{2.8}$$

$$c^2(\nabla F_t)^{-\top}\nabla v \cdot (\nabla F_t)^{-\top} n = 0 \text{ on } \sigma_0 \times (0,T), \tag{2.9}$$

$$c^2 \partial_n v = \hat{q} \text{ on } \Sigma_N, \tag{2.10}$$

$$v = 0 \text{ on } \Sigma_D, \tag{2.11}$$

$$v(x,0) = u_0(x) \text{ in } \Omega_0, \tag{2.12}$$

$$v_t(x,0) = u_1(x) + h'(0)\, \theta \cdot (\nabla F_t)^{-\top}\ \nabla v(x,0) = v_1(x) \text{ in } \Omega_0, \tag{2.13}$$

where

$$\begin{aligned} \mathcal{A}_0(t)v =& -\frac{c^2}{\det(\nabla F_t)} \div \left(\det(\nabla F_t)(\nabla F_t)^{-1}(\nabla F_t)^{-\top}\nabla v\right) \\ &+ h'^2\, \theta \cdot (\nabla F_t)^{-\top}\nabla\left(\theta \cdot (\nabla F_t)^{-\top}\nabla v\right), \\ \mathcal{A}_1(t)v =& h'^2\, \theta \cdot (\nabla F_t)^{-\top}(\nabla\theta)^{\top}(\nabla F_t)^{-\top}\nabla v \\ &- h''\, \theta \cdot (\nabla F_t)^{-\top}\nabla v, \\ \mathcal{B}(t)v_t =& -2h'\, \theta \cdot (\nabla F_t)^{-\top}\nabla v_t. \end{aligned}$$

Note that near the crack tip, where $\eta \equiv 1$, the operator $\mathcal{A}_0(t)$ reduces to the anisotropic Laplacian

$$\mathcal{A}_0(t) = -c^2(\alpha^2(t)\, \partial_1^2 + \partial_2^2),$$

where $\alpha^2(t) = 1 - \frac{h'(t)^2}{c^2}$.

In order to guarantee the ellipticity of $\mathcal{A}_0(t)$ we assume:

$$\exists \alpha_0 > 0 : 1 - \frac{h'(t)^2}{c^2} \geq \alpha_0^2 > 0, \forall t \in (0,T). \tag{2.14}$$

This assumption means that the crack velocity is not allowed to be faster than the wave speed.

In order to get the isotropic Laplacian we transform the space coordinates $x = (x_1, x_2)$ of Ω_0 into $z_1 = q_1(x,t)$, $z_2 = x_2$, where $z_1 = \frac{x_1}{\alpha(t)}$ near the crack tip. For details compare [22]. This last transformation has two advantages: We can apply the semigroup theory to the transformed initial-boundary value problem to get existence and solvability results and we can describe the

crack singularities in z-coordinates explicitly, namely $S_n(z_1, z_2) = \sqrt{r_z}\, \sin\frac{\phi_z}{2}$. The inverse transformations from the z-coordinates to the x-coordinates (reference configuration) and finally to the y-coordinates (actual configuration) lead the following result:

Theorem 2.1. [22]
Assume that (2.14) is satisfied and $h''(t)$ is uniformly bounded.
Let be

$$X_t = \left\{v \in H^2(\Omega_0) : c^2\partial_n v = \hat{q}\ on\, \Gamma_N \cup \sigma_0, v = 0\ on \Gamma_D\right\} \oplus \eta S_N$$

with the singular function

$$S_N(x_1, x_2, t) = \sqrt{\frac{r}{2\alpha(t)}}\sqrt{\sqrt{\cos^2\phi + \alpha^2(t)\sin^2\phi} - \cos\phi} \tag{2.15}$$

defined in the reference configuration.

For $\hat{f} \in Lip([0,T]; L^2(\Omega))$, $u_0 \in X_0$ and $u_1 \in L_2(\Omega)$, $\hat{q} \in \tilde{H}^{\frac{1}{2}}(\Gamma_N \times [0,T])$, there exists a unique solution $v \in C([0,T]; X_t) \cap C^1([0,T]; H^1(\Omega)) \cap C^2([0,T]; L^2(\Omega))$ of problem (2.8),. . . ,(2.13) in the configuration $\Omega_0 \times [0,T]$. If

$$u_0 = u_{R0} + k(0)\ \eta\ S_N(x_1, x_2, 0), \quad k(0) \in \mathbb{R},\ u_{R0} \in H^2(\Omega_0)$$
$$u_1 \in H^1_D(\Omega_0),$$

then the solution u admits the following decomposition into a regular part and a singular one in the actual configuration:

$$u(y,t) = u_R(y,t) + k(t,h,h')\eta(y)S_N(y_1 - h(t), y_2, t), \tag{2.16}$$

where the regular part u_R is in $C([0,T]; H^2(\Omega_t))$, $S_N(y_1 - h(t), y_2)$ is given by (1.3) and the stress intensity factor $k(t, h(t), h'(t))$ belongs to $C([0,T])$.

Furthermore,

$$\tilde{H}^{\frac{1}{2}}(\Gamma_N \times [0,T]) = \{u \in H^{1/2}(\Gamma \times (0,T)) : supp\ u \subset \overline{\Gamma_N} \times (0,T)\},$$
$$H^1_D(\Omega_0) = \{u \in H^1(\Omega_0) : u = 0\ on \Gamma_D\}.$$

Note that we have used the standard notation H^k for Sobolev spaces and C^j for spaces of continously differentiable functions.

In what follows we need explicitely the singular function S_N in the actual configuration. We denote both expressions by S_N and write the arguments to mark the regions where we are.

Lemma 2.2. *The singular function in the reference configuration (2.15) reads in the actual configuration*

$$S_N\left(y_1 - h, y_2, t\right) = \sqrt{\frac{1}{2\alpha\left(t\right)}}\sqrt{\sqrt{\left(R\cos\vartheta - h\right)^2 + \alpha^2\left(t\right)R^2\sin^2\vartheta} - \left(R\cos\vartheta - h\right)} \tag{2.17}$$

Here, (R, ϑ) are the actual polar coordinates with respect to the crack tip $(h(t), 0)$.

Proof: Let be $x_1 = r\cos\phi$, $x_2 = r\sin\phi$, $r = \sqrt{x_1^2 + x_2^2}$. We consider the (y_1, y_2)-coordinates in that region where the cut-off function $\eta \equiv 1$:

$$\begin{pmatrix} y_1 \\ y_2 \end{pmatrix} = \begin{pmatrix} R\cos\vartheta \\ R\sin\vartheta \end{pmatrix} = \begin{pmatrix} x_1 + h \\ x_2 \end{pmatrix} = \begin{pmatrix} r\cos\phi + h \\ r\sin\phi \end{pmatrix}. \tag{2.18}$$

Let us remark that $R = R(t), \vartheta = \vartheta(t), h = h(t)$. It follows

$$r\cos\phi = R\cos\vartheta - h, \quad r\sin\phi = R\sin\vartheta. \tag{2.19}$$

Inserting (2.19) into $S_N(x_1, x_2, t)$ given by (2.15) we get the relation (2.17).

The equation of motion for the running crack tip

In this section we will derive the equation of motion for the running crack tip (1.1) in a mathematic rigorous way. To this aim we start with the energy balance law in the actual configuration Ω_t:

$$\dot{D}(t) = -\dot{E}(t) + \hat{A}(t) - \dot{K}(t) \tag{2.20}$$

If $u = u(y,t)$ is a solution of problem (2.3), then

$$\dot{E}(t) = \frac{1}{2}\frac{d}{dt}\int\limits_{\Omega_t} c^2 |\nabla_y u(t,y)|^2 \, dy \tag{2.21}$$

is the rate of the elastic energy;

$$\hat{A}(t) = \int\limits_{\Omega_t} f u_t \, dy + \int\limits_{\Gamma_N} q u_t \, ds, \tag{2.22}$$

denotes the external energy and

$$\dot{K}(t) = \frac{d}{dt}\int\limits_{\Omega_t} \frac{1}{2}(u_t)^2 \, dy \tag{2.23}$$

is the rate of the kinetic energy.
D is the dissipative energy and it characterises the energy which is spent for irreversible processes. In our case the irreversible process is the breaking of bonds, the nucleation and growth of voids and micro-cracks in the process zone near the crack tip and the formation of a new macroscopic crack surface. In the simplest case the dissipative energy is considered in dependence on the fracture toughness and geometry properties. $\dot{D} = \frac{d}{dt}D$ is then the rate of dissipative energy.
The calculation of the expression $-\dot{E}(t) + \hat{A}(t) - \dot{K}(t)$ will be done by partial integration, the use of Gauss' divergence theorem and Reynolds transport theorem. Since the displacement field $u = u(y,t)$ developes crack singularities at the running crack tip we take a family of annular domains Ω_t^δ cutting out the running crack $h(t)$, see Fig.2 , and considering then the limit for $\delta \to 0$.

2.1. **The energy balance in the annular domain.** Let be $\Omega_t^\delta = \Omega_t \backslash \overline{M_t^\delta}$, where $\{M_t^\delta\}_\delta$ is a family of small neighborhoods of the running crack tip in the actual configuration such that $\lim_{\delta\to 0} M_t^\delta = \{h(t)\}$. We denote by C_t^δ the boundary curves of M_t^δ.

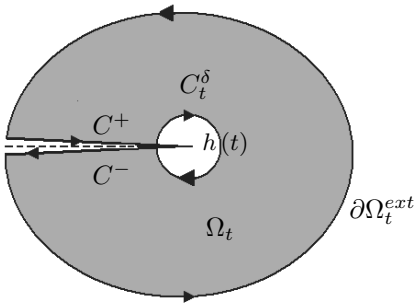

Figure 2: A family of annular domains cutting out the running crack $h(t)$.

We consider the energy flux in Ω_t^δ:

$$\dot{D}^\delta(t) = -\dot{E}^\delta(t) + \hat{A}^\delta(t) - \dot{K}^\delta(t) \tag{2.24}$$

where the energies are defined analogously to (2.20)-(2.23) as integrals on Ω_t^δ.
We remark that we use the notations $u_t = \dfrac{\partial u}{\partial t}$, $\dfrac{\partial}{\partial t} = \partial_t$.

Lemma 2.3. *The following identity holds:*

$$\hat{A}^{\delta}(t) - \dot{E}^{\delta}(t) - \dot{K}^{\delta}(t) = -\frac{1}{2}\int_{\Omega_t^{\delta}} \div_y[\left(u_t^2 + c^2|\nabla u|^2\right)\frac{\partial y(t)}{\partial t}]\, dy - \int_{C_t^{\delta}} c^2\,\frac{\partial u}{\partial n}\,\partial_t u\, ds_y. \tag{2.25}$$

where $y(t) = y(x,t) = F_t(x) = x + h(t)\,\theta(x)$ and the scalar field u solves the initial boundary value problem (2.3).

Proof
We start with the wave equation

$$\partial_t^2 u - c^2\Delta u = f \quad \text{in} \quad \Omega_t \tag{2.26}$$

and consider the restriction u^{δ} of u to Ω_t^{δ}. We remark that u^{δ} is smooth enough in Ω_t^{δ} in order to apply partial integration and the formula of Gauss. Multiplication of (2.26) with $\partial_t u^{\delta}$ and integration on Ω_t^{δ} yield

$$\begin{aligned}
&\int_{\Omega_t^{\delta}} \left(\partial_t^2 u^{\delta}\;\partial_t u^{\delta} - c^2\;\Delta u^{\delta}\;\partial_t u^{\delta}\right) dy = \\
&\int_{\Omega_t^{\delta}} \left(\frac{1}{2}\frac{\partial}{\partial t}\left(u_t^{\delta 2}\right) + c^2\;\nabla u^{\delta}\;\nabla\partial_t u^{\delta}\right) dy - \int_{\partial\Omega_t^{\delta}} c^2\,\frac{\partial u^{\delta}}{\partial n}\,\partial_t u^{\delta}\, ds_y = \int_{\Omega_t^{\delta}} f\;\partial_t\;u^{\delta}\, dy.
\end{aligned}$$

Therefore

$$\begin{aligned}
&\int_{\Omega_t^{\delta}} \frac{1}{2}\left(\frac{\partial}{\partial t}\left(u_t^{\delta 2}\right) + c^2\frac{\partial}{\partial t}\left(\nabla u^{\delta}\right)^2\right) dy = \\
&\int_{\Omega_t^{\delta}} f\;\partial_t u^{\delta}\, dy + \int_{\partial\Omega_t^{ext}} c^2\,\frac{\partial u^{\delta}}{\partial n}\,\partial_t u^{\delta}\, ds_y + \int_{C_t^{\delta}} c^2\,\frac{\partial u^{\delta}}{\partial n}\,\partial_t u^{\delta}\, ds_y
\end{aligned} \tag{2.27}$$

From Reynolds' transport theorem follows (here we set $u^{\delta} = u$ in Ω_t^{δ}):

$$\begin{aligned}
&\dot{E}^{\delta}(t) + \dot{K}^{\delta}(t) = \frac{d}{dt}\frac{1}{2}\int_{\Omega_t^{\delta}} \left[(\partial_t u)^2 + c^2|\nabla u|^2\right] dy \\
&= \frac{1}{2}\int_{\Omega_t^{\delta}} \frac{\partial}{\partial t}(\partial_t u)^2 + \frac{\partial}{\partial t}c^2|\nabla u|^2\, dy + \frac{1}{2}\int_{\Omega_t^{\delta}} \operatorname{div}\left[\left((\partial_t u)^2 + c^2|\nabla u|^2\right)\frac{\partial y}{\partial t}\right] dy \\
&= \int_{\Omega_t^{\delta}} f\;\partial_t u\, dy + \int_{\Gamma_N} q\;\partial_t u\, ds_y + \int_{C_t^{\delta}} c^2\,\frac{\partial u}{\partial n}\,\partial_t u\, ds_y + \\
&+ \frac{1}{2}\int_{\Omega_t^{\delta}} \operatorname{div}\left[\left((\partial_t u)^2 + c^2|\nabla u|^2\right)\frac{\partial y}{\partial t}\right] dy \\
&= \hat{A}^{\delta}(t) + \frac{1}{2}\int_{\Omega_t^{\delta}} \operatorname{div}\left[\left((\partial_t u)^2 + c^2\,|\nabla u|^2\right)\frac{\partial y}{\partial t}\right] dy + \int_{C_t^{\delta}} c^2\,\frac{\partial u}{\partial n}\,\partial_t u\, ds_y
\end{aligned}$$

We have used (2.27). It follows (2.25).

Remark 2.1. *The family of smooth neighborhoods of $h(t)$, $\{M_t^{\delta}\}$, in the actual configuration is chosen in such a way that their images $\{F_t^{-1}\left(M_t^{\delta}\right)\}_{\delta}$ are circles B_{δ} with radius δ around the crack tip $\{0\}$ in the reference configuration.*

2.2. **The limit procedure $\delta \to 0$.** We calculate the limit for $\delta \to 0$ of the right hand side of (2.25) transforming both integrals to the reference domain $\Omega^{\delta} = \Omega\backslash\overline{B_{\delta}}$.

Lemma 2.4. *For the right hand side of (2.25) holds:*

$$\begin{aligned}
&\lim_{\delta\to 0}\{-\frac{1}{2}\int_{\Omega_t^\delta} \div_y[\left(u_t^2+c^2\,|\nabla u|^2\right)\frac{\partial y\,(t)}{\partial t}]\,dy\}+\lim_{\delta\to 0}\{-\int_{C_t^\delta} c^2\,\frac{\partial u}{\partial n}\,\partial_t u\,ds_y\}\\
&=h'(t)\;k^2(t,h,h')\;c^2\;\frac{\pi}{4}\;\frac{(\alpha-1)}{\alpha}+h'(t)\;k^2\,(t,h,h')\;\;c^2\;\frac{\pi}{4}\;\frac{1}{\alpha}\\
&=h'(t)\;k^2(t,h,h')\;c^2\;\frac{\pi}{4}.
\end{aligned}\tag{2.28}$$

Proof
We start with the integral

$$\begin{aligned}
I_1^\delta&=-\frac{1}{2}\int_{\Omega_t^\delta}\mathrm{div}_y\left(\left(u_t^2+c^2|\nabla u|^2\right)\frac{\partial y(t)}{\partial t}\right)dy\\
&=-\frac{1}{2}\int_{\partial\Omega_t^\delta} n_y\cdot\left(u_t^2+c^2|\nabla u|^2\right)\;\frac{\partial y(t)}{\partial t}\,ds_y.
\end{aligned}\tag{2.29}$$

We transform the boundary integral (2.29) to the boundary of the reference configuration $\partial\Omega^\delta$. We recall that

$$y=\begin{pmatrix}x_1\\x_2\end{pmatrix}+h\,(t)\begin{pmatrix}\eta\,(x)\\0\end{pmatrix},$$

where η is a cut-off function with support in a neighborhood of the crack tip $\{0\}$. After some elementary calculations, see [22], we get

$$\begin{aligned}
I_1^\delta=&-\frac{1}{2}\int_{\partial\Omega^\delta} n_{x_1}\left(\partial_t v-\frac{h'\eta\partial_1 v}{1+h\partial_1\eta}\right)^2 h'(t)\;\eta\;ds_x+\\
&-\frac{1}{2}\int_{\partial\Omega^\delta} n_{x_1}\left(\frac{c^2}{\left(1+h\partial_1\eta\right)^2}\left(\left(\partial_1 v\right)^2+\left(-\partial_1 v h\partial_2\eta+\partial_2 v\,(1+h\partial_1\eta)\right)^2\right)\right)h'(t)\eta ds_x.
\end{aligned}$$

Note that η vanishes on $\partial\Omega_\delta^{ext}$ and that the first component $n_{x_1}=n_1$ of the normal vector vanishes on the crack $\sigma_0^{\pm}$. Therefore, we have

$$\begin{aligned}
I_1=\lim_{\delta\to 0} I_1^\delta=\lim_{\delta\to 0}-\frac{1}{2}\int_{\partial B_\delta} n_1\left([\partial_t v-\frac{h'\eta\partial_1 v}{1+h\partial_1\eta}]^2 h'\,(t)\,\eta\right)ds_x+\\
\lim_{\delta\to 0}-\frac{1}{2}\int_{\partial B_\delta} n_1\left(\frac{c^2}{\left(1+h\partial_1\eta\right)^2}\left(\left(\partial_1 v\right)^2+\left(-\partial_1 v h\partial_2\eta+\partial_2 v\,(1+h\partial_1\eta)\right)^2\right)\right)h'(t)\eta ds_x.
\end{aligned}$$

We assume that δ is so small that $\eta\equiv 1$ on $\overline{B_\delta}$. Furthermore, we use the asymptotic expansion of v on ∂B_δ:

$$v\,(x,t)=v_R\,(x,t)+k\,(t,h,h')\,S_N(x_1,x_2,t)=v_R+\widehat{v}_S,\tag{2.30}$$

where S_N is given by theorem 2.1, namely

$$S_N(x_1,x_2,t)=\sqrt{\frac{r}{2\alpha(t)}}\sqrt{\sqrt{\cos^2\varphi+\alpha(t)^2\sin^2\varphi}-\cos\varphi}=\sqrt{\frac{r}{2\alpha(t)}}v_s.$$

Due to the fact that the limit value of the integrals on expressions of v_R vanishes, we get the simplified relation:

$$I_1=\lim_{\delta\to 0}-\frac{1}{2}\,h'(t)\;\delta\int_{-\pi}^{\pi}\left[n_1\left(\partial_t\widehat{v}_S-h'\partial_1\widehat{v}_S\right)^2+n_1c^2\left(\partial_1\widehat{v}_S^2+\partial_2\widehat{v}_S^2\right)\right]ds$$

Since $n_1=-\cos\phi$ it follows

$$I_1=\lim_{\delta\to 0}h'(t)\;\delta\int_0^{\pi}\left[\cos\phi\;\left(\partial_t\widehat{v}_S-h'\partial_1\widehat{v}_S\right)^2+c^2\cos\phi\;\left(\partial_1\widehat{v}_S^2+\partial_2\widehat{v}_S^2\right)\right]ds.\tag{2.31}$$

The singular function S_N behaves with respect to δ as follows:

$$S_N \sim \delta^{\frac{1}{2}}, \quad \partial_t S_N \sim \delta^{\frac{1}{2}}, \quad \partial_1 S_N \sim \delta^{-\frac{1}{2}}, \quad \partial_2 S_N \sim \delta^{-\frac{1}{2}}$$

It follows from (2.31)

$$\begin{aligned} I_1 &= \lim_{\delta\to 0} h'(t)\; k^2(t,h,h')\; \delta \int_0^\pi \cos\phi \left[\left(h'(t)^2 + c^2\right) \left(\partial_1 S_N\right)^2 + c^2 \left(\partial_2 S_N\right)^2 \right] d\phi \\ &= \lim_{\delta\to 0} h'(t)\; k^2(t,h,h')\; c^2\; \delta \int_0^\pi \cos\phi \left[\left(2 - \alpha(t)^2\right) \left(\partial_1 S_N\right)^2 + \left(\partial_2 S_N\right)^2 \right] d\phi. \end{aligned} \tag{2.32}$$

Since

$$\begin{aligned} \left(\partial_1 S_N\right)^2 &= \left[\frac{\partial S_N}{\partial r} \cos\phi - \frac{1}{r} \frac{\partial S_N}{\partial \phi} \sin\phi \right]^2 = \frac{1}{2\alpha r} \left[\frac{1}{2} v_s \cos\phi - \frac{\partial v_s}{\partial \phi} \sin\phi \right]^2 \\ \left(\partial_2 S_N\right)^2 &= \left[\frac{\partial S_N}{\partial r} \sin\phi + \frac{1}{r} \frac{\partial S_N}{\partial \phi} \cos\phi \right]^2 = \frac{1}{2\alpha r} \left[\frac{1}{2} v_s \sin\phi + \frac{\partial v_s}{\partial \phi} \cos\phi \right]^2 \end{aligned} \tag{2.33}$$

we have

$$\begin{aligned} &\lim_{\delta\to 0} \delta \int_0^\pi \cos\phi \left[\left(2 - \alpha^2(t)\right) \left(\partial_1 S_N\right)^2 + \left(\partial_2 S_N\right)^2 \right] d\phi \\ &= \frac{1}{2\alpha} \int_0^\pi \left[\frac{1}{4} v_s^2 \left(1 - \alpha^2\right) \cos^3\phi + \frac{1}{4} v_s^2 \cos\phi + \left(\frac{\partial v_s}{\partial \phi} \right)^2 \left(\alpha^2 - 1\right) \cos^3\phi \right] + \\ &+ \frac{1}{2\alpha} \int_0^\pi \left[\left(2 - \alpha^2\right) \left(\frac{\partial v_s}{\partial \phi} \right)^2 \cos\phi + \left(\alpha^2 - 1\right) \cos^2\phi \sin\phi v_s \frac{\partial v_s}{\partial \phi} \right] d\phi. \end{aligned}$$

Furthermore, we easily check that

$$\begin{aligned} J &= \int_0^\pi \cos^2\phi\; \sin\phi\; v_s\; \frac{\partial v_s}{\partial \phi}\; d\phi \\ &= -\int_0^\pi \left[-2\; \cos\phi\; \sin^2\phi\; v_s + \cos^3\phi\; v_s + \cos^2\phi\; \sin\phi\; \frac{\partial v_s}{\partial \phi} \right] v_s\; d\phi \\ &= \int_0^\pi \left(2\; \cos\phi \left(1 - \cos^2\phi\right) v_s^2 - \cos^3\; \phi v_s^2 \right) - J, \end{aligned}$$

or equivalently

$$J = \int_0^\pi \left(\cos\phi\; v_s^2 - \frac{3}{2} \cos^3\phi\; v_s^2 \right)\; d\phi.$$

The expressions of v_s^2 and of $\left(\frac{\partial v_s}{\partial \phi} \right)^2$ read:

$$\begin{aligned} \left(v_s\right)^2 &= \sqrt{\cos^2\phi + \alpha^2(t) \sin^2\phi} - \cos\phi = \text{symmetric part} - \cos\phi, \\ \left(\frac{\partial v_s}{\partial \phi} \right)^2 &= \frac{1}{4\left(\cos^2\phi + \alpha^2(t)\sin^2\phi\right)} \left[\sqrt{\cos^2\phi + \alpha^2(t)\sin^2\phi} \left(\left(\alpha^2(t) - 1\right) \cos^2\phi + 1 \right) \right] \\ &\quad + \frac{1}{4} \cos\phi \left(1 + \frac{\alpha^2(t) - 1}{\cos^2\phi + \alpha^2(t)\sin^2\phi} \right) \\ &= \text{symmetric part} + \frac{1}{4} \cos\phi \left(1 + \frac{\alpha^2(t) - 1}{\cos^2\phi + \alpha^2(t)\sin^2\phi} \right). \end{aligned} \tag{2.34}$$

Both terms consist of a symmetric and an odd part with part respect to $\frac{\pi}{2}$ and the odd parts contribute to the integral I_1 only.
Inserting these expressions into (2.32) and taking the limit value for $\delta \to 0$, we get

$$I_1 = h'(t)\; k^2(t,h,h')\; c^2\; \frac{\pi}{4}\; \frac{(-1 + \alpha(t))}{\alpha(t)}$$

Here we have used that

$$\int_0^\pi \frac{\cos^2\phi}{\cos^2\phi+\alpha^2(t)\sin^2\phi}d\phi = \pi\,\frac{1}{1+\alpha(t)},$$
$$\int_0^\pi \frac{\cos^4\phi}{\cos^2\phi+\alpha^2(t)\sin^2\phi}\,d\phi = \frac{\pi}{2}\,\frac{1+2\alpha(t)}{(1+\alpha(t))^2}.$$

Now we consider the second integral of (2.28)

$$I_2^\delta = -\int_{C_t^\delta} c^2\,\frac{\partial u}{\partial n}\,\partial_t u\,ds_y.$$

We transform it to the reference configuration. Since

$$\frac{\partial u}{\partial n_y} = \nabla_y u\cdot n_y = (\nabla F_t)^{-T}\nabla_x v\cdot\frac{(\nabla F_t)^{-T}n_x}{|\,(\nabla F_t)^{-T}n_x|},$$
$$\partial_t u = \partial_t v - h'\theta\cdot(\nabla F_t)^{-T}\nabla_x v$$

and δ is so small that, $\eta\equiv 1$ on $\overline{B_\delta}$ it follows

$$I_2^\delta = -c^2\int_{\partial B^\delta}\nabla_x v\cdot\frac{n_x}{|n_x|}\,(\partial_t v - h'\partial_1 v)\,\mathrm{ds}_x \tag{2.35}$$

Since $n_x = -\begin{pmatrix}\cos\phi\\ \sin\phi\end{pmatrix}$, we get from (2.35)

$$I_2 = \lim_{\delta\to 0} I_2^\delta = \lim_{\delta\to 0} c^2\,\delta\int_{\partial B^\delta}(\partial_1 v\ \cos\phi+\partial_2 v\ \sin\phi)\,(\partial_t v - h'\ \partial_1 v)\,d\phi. \tag{2.36}$$

As before we split v, $v = v_R+\widehat{v}_S$, compare (2.30), and repeat the arguments for the behaviour of the terms v_R and $\widehat{v}_S$ with respect to δ. Furthermore, we use the formulas (2.33).

Then (2.36) can be written as:

$$\begin{aligned} I_2 =& -\frac{c^2h'(t)k^2\,(t,h,h')}{\alpha(t)}\int_0^\pi\left(\frac{1}{2}v_s\cos\phi-\frac{\partial v_s}{\partial\phi}\sin\phi\right)\left(\frac{1}{2}v_s\cos\phi-\frac{\partial v_S}{\partial\phi}\sin\phi\right)\cos\phi+\\ &+\left(\frac{1}{2}\ v_s\ \sin\phi+\frac{\partial v_s}{\partial\phi}\ \cos\phi\right)\ \sin\phi\,d\phi \\ =& -\frac{c^2h'\,(t)\,k^2\,(t,h,h')}{\alpha(t)}\int_0^\pi\left(\frac{1}{2}\ v_s\cos\phi-\frac{\partial v_s}{\partial\phi}\ \sin\phi\right)\frac{1}{2}\ v_s\ d\phi. \end{aligned} \tag{2.37}$$

Since

$$(v_s)^2 = \sqrt{\cos^2\phi+\alpha^2(t)\ \sin^2\phi}-\cos\phi,$$
$$\frac{d}{d\phi}(v_s)^2 = 2\ v_s\ \frac{\partial v_s}{\partial\phi} = \frac{\left(\alpha^2(t)-1\right)\cos\phi\ \sin\phi}{\sqrt{\cos^2\phi+\alpha^2(t)\sin^2\phi}}+\sin\phi,$$

it follows that

$$\frac{\partial v_s}{\partial\phi}\ v_s\ \sin\phi = \frac{\left(\alpha^2(t)-1\right)\cos\phi\ \sin^2\phi}{2\sqrt{\cos^2\phi+\alpha^2(t)\ \sin^2\phi}}+\frac{\sin^2\phi}{2}.$$

Again, only the odd term with respect to $\frac{\pi}{2}$ contribute to the integral (2.37). Therefore,

$$\begin{aligned} I_2 &= -\frac{c^2\ h'(t)\ k^2(t,h,h')}{\alpha(t)} \int_0^\pi \left(-\frac{1}{4}\ \cos^2\phi - \frac{1}{2}\ \frac{\sin^2\phi}{2}\right) d\phi \\ &= \frac{c^2\ h'(t)\ k^2(t,h,h')}{\alpha(t)} \left(\frac{\pi}{8} + \frac{\pi}{8}\right) \\ &= \frac{c^2\ h'(t)\ k^2(t,h,h')}{\alpha(t)}\ \frac{\pi}{4} \end{aligned}$$

and the relation (2.28) follows.

Remark 2.2. *Lemmata 2.3 and 2.4 yield*

$$\lim_{\delta\to 0}\left(-\dot{E}^\delta(t) + \hat{A}^\delta(t) - \dot{K}^\delta(t)\right) = \lim_{\delta\to 0}\dot{D}^\delta(t) = c^2\ h'(t)\ k^2(t,h,h')\ \frac{\pi}{4}.$$

From the other side the energy flux in Ω_t, namely $-\dot{E}(t) + \hat{A}(t) - \dot{K}(t)$, is well defined, at least in the distribution sense (compare Theorem 2.1). We conclude that

$$\begin{aligned} -\dot{E}(t) + \hat{A}(t) - \dot{K}(t) &= \lim_{\delta\to 0}\left(-\dot{E}^\delta(t) + \hat{A}^\delta(t) - \dot{K}^\delta(t)\right) \\ &= \dot{D}(t) = c^2\ h'(t)\ k^2(t,h,h')\ \frac{\pi}{4}. \end{aligned}$$

In books about crack mechanics, [4, 12, 14], can be found the following formula for the dynamic energy release rate for $h'(t) \neq 0$:

$$\frac{\dot{D}(t)}{h'(t)} = \frac{1}{2\mu}\frac{\widehat{K}^2\,(t,h,h')}{\alpha(t)}, \tag{2.38}$$

where μ is the Lamé coefficient, $\alpha(t) = \sqrt{1 - \frac{h'^2(t)}{c^2}}$ and $\widehat{K}(t,h,h')$ represents the stress intensity factor.
It should be then:

$$\begin{aligned} c^2\ k^2(t,h,h')\ \frac{\pi}{4} &= \frac{1}{2\ \mu}\ \frac{\widehat{K}^2(t,h,h')}{\alpha(t)}, \\ k^2(t,h,h') &= \frac{2}{\pi}\ \frac{1}{\mu\ c^2}\ \frac{\widehat{K}^2(t,h,h')}{\alpha(t)}, \\ k(t,h,h') &= \sqrt{\frac{2}{\pi\ \mu}}\ \frac{1}{c}\ \frac{\widehat{K}(t,h,h')}{\sqrt{\alpha(t)}}. \end{aligned}$$

Indeed, the singular function w_{sing} in the z-coordinates, is here written as:

$$w_{sing} = k(t,h,h')\ \sqrt{r_z}\ \sin\frac{\phi_z}{2} = k(t,h,h')\ S_N(z,t), \tag{2.39}$$

whereas

$$\widehat{w}_{sing} = \frac{\widehat{K}(t,h,h')}{\alpha(t)\ \mu}\sqrt{\frac{2}{\pi}}\ \sqrt{r_z}\ \sin\frac{\phi_z}{2} = \widehat{K}(t,h,h')\ \widehat{S}_N(z,t) \tag{2.40}$$

is used in mechanics, in order to get formula (2.38).

Assuming that the dynamic energy release rate can be expressed by the experimentally determined fracture toughness [12], $\Gamma(h,h')$, we get the ordinary differential equation

$$\Gamma(h,h') = k^2(t,h,h')\ c^2\ \frac{\pi}{4}. \tag{2.41}$$

It follows the initial problem (1.1) which is basic for the computation of the motion $h(t)$ of the crack tip.
Note that the quasistatic case, $h'(t) = 0$, is included in (2.41).

3. Numerical simulations

3.1. **Some basics.** In this subsection we derive some expressions from the analytical results, which are necessary for the numerical computations. In particular, we prepare the numerical extraction of the the dynamical stress intensity factors $k(t,h,h')$ at time t from the actual displacement field decomposition (2.16).

Theorem 3.1. *Assume that theorem 2.1 holds, that means, the solution $u(y,t)$ of (2.3) can be decomposed as*

$$u(y,t) = u_R(y,t) + k(t,h,h')\eta(y)S_N(y_1 - h(t), y_2, t)$$

where S_N is given by (2.17). Then the stress intensity factor $k(t,h,h')$ at time t can be found for $R(t) - h(t) > 0$ as the limit

$$\lim_{R(t)-h(t)\to 0} \frac{2}{\sqrt{\alpha(t)}}\sqrt{(R(t)-h(t))}\frac{\partial u}{\partial y_2}|_{\vartheta=0} = k(t,h,h'). \tag{3.1}$$

Proof: Since u can be represented as

$$u(y,t) = u_R(y,t) + k(t,h,h')\eta(y)\sqrt{\frac{1}{2\,\alpha\,(t)}}\sqrt{\sqrt{(y_1-h)^2 + \alpha^2\,(t)\,y_2^2} - (y_1-h)}$$

we calculate $\frac{\partial u}{\partial y_2}|_{\vartheta=0}$ in a vicinity of the crack tip where $\eta \equiv 1$. We get there

$$\frac{\partial u}{\partial y_2}|_{\vartheta=0} = \frac{\partial u_R}{\partial y_2}|_{\vartheta=0} + k(t,h,h')\frac{\sqrt{\alpha}}{2\sqrt{R-h}} \tag{3.2}$$

Here we have used the fact, compare (2.34), that

$$\frac{\partial S_N}{\partial y_2}|_{\vartheta=0} = \frac{\partial S_N}{\partial x_2}|_{\phi=0} = \frac{1}{\sqrt{2\alpha r}}\frac{\partial v_s}{\partial \phi}|_{\phi=0} = \frac{\sqrt{\alpha}}{2\sqrt{r}}.$$

Furthermore, we have $r = R - h$ on the y_1-axis assuming $R > h$. Multiplying (3.2) by $\frac{2\sqrt{R-h}}{\sqrt{\alpha}}$ and using the fact that the derivative of the regular part $\frac{\partial u_R}{\partial y_2}$ behaves in a vicinity of the crack tip asymptotically as $\sqrt{R-h}$ the assertion (3.1) follows.

3.2. **Basic concepts and remarks on the implementation.** We discuss some basic concepts of the numerical simulation, namely the software components and environments which are used in the following.
We present simulations in two space dimensions only. For that reason we deal with meshes consisting of triangles using the software package PDE2D. PDE2D approximates the solution using a linear combination of piecewise polynomial basis functions, where the unknown coefficients are functions of time. A Galerkin finite element method is used, which results in a system of ordinary differential equations for the unknown coefficient functions; this differential equation system is solved using a finite difference method.
The last task of the simulation process is the visualization of the computed data. PDE2D generates its own graphics, in PostScript format, and also generates a MATLAB program which can be used to create further plots.
Finally, we apply GNUPlot in order to visualise scalar valued data like displacement field, dynamic stress intensity factor and energy. GNUPlot is free software, which can be downloaded from [37].

3.2.1. ***General setting of the simulations.*** The following simulations are performed in a situation where a square with side length of $2\,m$ with an interior crack on the right side is considered. This domain is clamped at one side, describing the Dirichlet boundary part. The remaining boundary denotes the Neumann part, whereas the loads are described later for the individual examples. A final triangulation is shown in Fig.3(a) and the corresponding zoom of the cracked zone in Fig.3(b). We focus on the numerical simulation of the coupled problem (2.3) and (1.1). The material parameters used in the following computations and the different pre-conditions on the equation of motion are presented here.

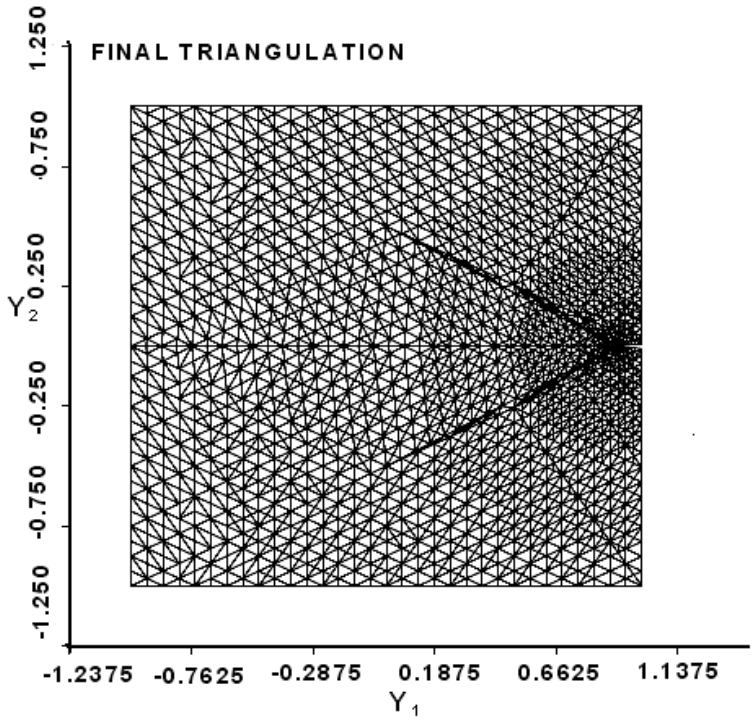

a)

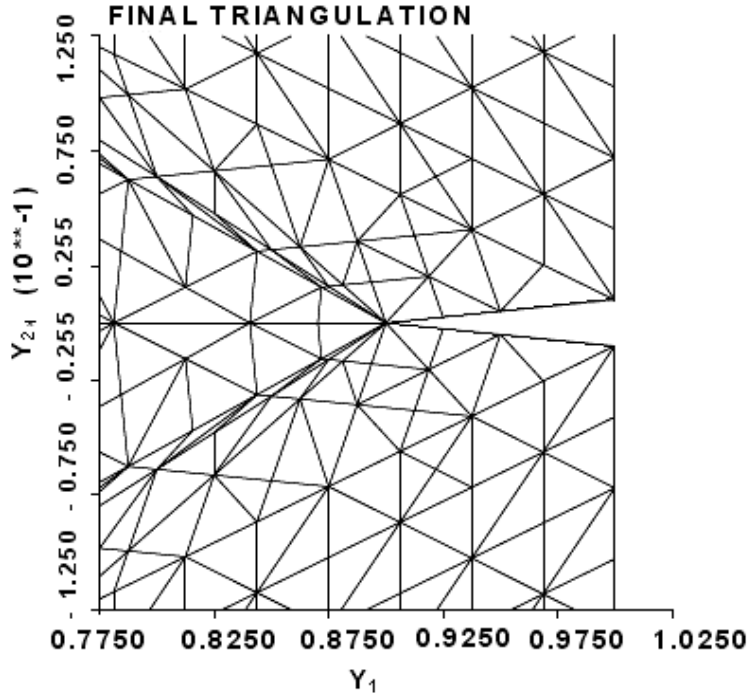

b)

Figure 3: Computational domains

To predict the crack path $h = h(t)$ by numerical calculation, one has to calculate the displacement field at the points arround the crack tip, from which the corresponding dynamic stress intensity factor is subsequently extracted. One then repeats this process incrementally.

3.2.2. ***Iterative solution strategy.*** The following iterative procedure to solve the nonlinear coupled problem is proposed here:

(1) Fix $t_0 > 0$ and a time step τ, and set $t_{-1} = 0$, and assume $h(t) = h_0(t)$ is known for $t_{-1} < t < t_0$.
(2) Solve the initial boundary value problem (2.3) for the wave equation for $t_{-1} < t < t_0$ in the cracked domain with the given straight crack-path $h_0(t)$.
(3) Extract the corresponding dynamical stress intensity factor $k(t_0, h_0, h_0')$ by the formula (3.1).
(4) Insert $k(t_0, h_0, h_0')$ into (1.1), use an experimentally chosen formula for $\Gamma(h, h')$ and solve the resulting ordinary differential equation for $h(t)$ with the initial datum $h(t_0) = h_0(t_0)$. Denote the solution by $h_1(t), t \in (t_0, t_0 + \tau)$.
(5) Go to step 2 and replace $h_0(t), t_{-1}, t_0$ respectively by $h_1(t), t_0, t_0 + \tau$.

The computational domain consists of a cracked, finite, homogeneous, isotropic and linearly elastic solid, which is described by the square R with vertices (-1,-1),(1,-1),
(1,1) and (-1,1) and an interior crack σ_{t_0} from $(h(t_0), 0)$ to (1,0) along the y_1-axis. The crack σ_{t_0} interacts with an incident transient elastic wave, whose front is assumed to be planar. The interaction between the incident wave and the crack forms an initial boundary value problem, which is described by equations (2.3). Its solution is performed numerically by using the software PDE2D to describe the local behavior of the displacement fields near the crack tip $h(t)$.
The material properties of the square plate are assumed to include elastic modulus $E = 68.9GPa$, Poisson's ratio $\nu = 0.3$, mass density $\rho = 2.77(10)^3 Kg/m^3$, Lamé parameter $\mu = 2.7(10)^{10} N/m^2$ and shear wave speed $c = \sqrt{\dfrac{E}{2\rho(1+\nu)}} = 3093m/s$, [6].

Typical finite element analysis in dynamic fracture mechanics problems for crack propagation involves as a first step, the construction of a mesh appropriate for the crack geometry. Moreover, when the crack evolves, the mesh should evolve also and must conform to the crack geometry. As the crack is part of the mesh, this involves the update of the mesh, as well as the data structure associated with the crack geometry. Hence one must treat a moving-singularity-boundary-value-problem and the moving singularity induces various errors in numerical methods.

Therefore the dump/restart option from PDE2D [25] has been used. This option in PDE2D is useful for this problem because it makes it easy to stop at some value of the time t, adjust the grid or even the boundary appropriately, and restart. The grids are generated automatically and adaptively moved with the solution, by putting a "DO loop" around the main program to vary the initial and final time values each pass, and requesting a restart with an adaptively determined grid.

The initial conditions have been read from the restart file each time and then PDE2D dumps the final solution at the end of each run back into the restart file, [25]. 4000 elements of degree 2 have been used for the final triangulation and the adaptively generated grids are most dense near the crack tip. The corresponding spatial discretization error is $O(h^3)$, where h is the maximum triangle diameter.
The time increment Δt has been chosen as $\Delta t = 0.00003$ s. The time discretization used is the Crank-Nicolson scheme, [25].

The iterative numerical technique proposed here was used in the numerical simulation to find the unknowns (u, h). This technique requires additional computing time because of the nature of the iteration. Because of that the MPI-based parallel band solver implemented in PDE2D [25] was

used. This is a parallel solver which runs efficiently on multiple processor machines, in our cases 6 processors were used, with the matrix distributed over the available processors.

3.2.3. ***Order reduction for the time-dependent problem.*** There are no body forces, $f = 0$, and the problem (2.3) is broken into two first order equations [34] before it can be solved by PDE2D [25]. The form of the 2D time-dependent system solved by PDE2D [25] is:

$$\begin{aligned} C_{11} * \frac{\partial U}{\partial T} + C_{12} * \frac{\partial V}{\partial T} &= \frac{\partial A_1}{\partial y_1} + \frac{\partial B_1}{\partial y_2} - F_1 \\ C_{21} * \frac{\partial U}{\partial T} + C_{22} * \frac{\partial V}{\partial T} &= \frac{\partial A_2}{\partial y_1} + \frac{\partial B_2}{\partial y_2} - F_2 \end{aligned} \tag{3.3}$$

where all coefficients can be functions of y_1, y_2, T, U, V and the derivatives of U and V.
We set the following functions in (3.3):

$$\begin{aligned} &C_{11} = 1; \quad C_{12} = 0; \quad F1 = -V; \quad A_1 = 0; \quad B_1 = 0 \\ &C_{21} = 0; \quad C_{22} = 1; \quad F2 = 0; \quad A_2 = c^2 * Uy_1; \quad B_1 = c^2 * Uy_2 \end{aligned}$$

and the order reduction of (2.3) results.

3.2.4. ***Simulation of dynamic stress intensity factor.*** As we pointed out, the crack propagation is simulated by remeshing the whole spatial domain each time increment so that the mesh is always highly refined near the crack-tip.

The computation of stress intensity factors must be carefully done since the evolution of the crack depends on that. Numerical calculations for $k(t, h, h')$ have been carried out in the following way:

- A regular $(N_{y_1} + 1)$ by $(N_{y_2} + 1)$ rectangular output grid is used for the discretization of the square configuration, consisting of the points:
  $\left(Y_{1_A} + i * \frac{(Y_{1_B} - Y_{1_A})}{N_{y_1}}, Y_{2_A} + j * \frac{(Y_{2_B} - Y_{2_A})}{N_{y_2}}\right)$,
  where $i = 0, ..., N_{y_1}$ and $j = 0, ..., N_{y_2}$ and $Y_{1_A} = -1$, $Y_{1_B} = h\,(t)$, $Y_{2_A} = -1$ and $Y_{2_A} = 1$.
- The function $\frac{2}{\sqrt{\alpha}}\sqrt{(R - h_0(t_0))}\frac{\partial u}{\partial y_2}$ is output at all grid points.
- To estimate the limit in formula (3.1) we simply use the value of this function at the last output grid point in front of the crack tip, $(N_{y_1} - 1, \frac{N_{y_2}}{2})$.

Thus the point where the dynamic stress intensity is evaluated is $(N_{y_1} = N_{y_2} = 60)$:

$$(-1 + (N_{y_1} - 1) * \frac{(h(t) + 1)}{N_{y_1}}\ , -1 + \frac{N_{y_2}}{2} * \frac{2}{N_{y_2}}) = (h(t) - \frac{1}{60} * (h(t) + 1)\ , 0).$$

This is the output grid point closest to, and in front of the crack tip. The finite element grid is refined locally in such a way as to ensure that there are several triangles between this point and the crack tip, so that reasonable accuracy can be expected at this point.

The values of $\frac{\partial u}{\partial y_2}$ at the grid points, from which the dynamic stress intensity factors are subsequently extracted, are computed by PDE2D using exact differentiation of its piecewise polynomial approximation to u.

3.2.5. ***The fracture toughness*** $\Gamma(h, h')$. The time history of the dynamic stress intensity factor was obtained for different situations and $h(t)$ was calculated using the generalised equation of motion, the formula (1.1)

$$\Gamma(h, h') = k^2(t, h, h')c^2\frac{\pi}{4}, \quad h(0) = 0$$

which includes the situation where the crack propagates with non-uniform speed.

The parameter Γ appearing on the left-hand side of the equation of motion (1.1) is the fracture toughness; it is a material parameter which can only be obtained through experimental measurements [17], [29], and it represents the resistance of the material to the advance of the crack. On the right-hand side appears the dynamic stress intensity factor $k(t, h, h')$, which is entirely determined through an analysis of the boundary/initial value problem, see (3.1).

In the following simulations, we assume the following formula for the fracture toughness:

$$\Gamma(h, h') = \beta * \frac{1 - \alpha(t)}{\alpha(t)} \tag{3.4}$$

with $\alpha(t)$ defined as in (1.4), and $\beta = 36\,\mathrm{MPa}/m^{\frac{1}{2}}$. More details about β, see e.g. [35],[36].

We have unfortunately no experimental justification for this or any other formula for $\Gamma(h, h')$, this formula was chosen because it produces qualitatively reasonable results, in particular, when $k = 0, h'(t) = 0$ and when k^2 is large, $h'(t)$ approaches c. Nevertheless, the software developed in this paper can be easily adapted to experimentally justified fracture toughness formulas, when such are available. From (3.4) we get:

$$\frac{1 - \alpha}{\alpha} = k^2(t, h, h') \left(\frac{c^2}{\beta}\right) \frac{\pi}{4}.$$

Simple calculations lead to:

$$h'(t) = c\sqrt{1 - \left(\frac{1}{1 + TMP}\right)^2} \tag{3.5}$$

where $TMP(t, h, h') = k^2(t, h, h') \left(\frac{c^2}{\beta}\right) \frac{\pi}{4}$, and c^2 and β have the same order of magnitude.

3.3. **Setting.** Two examples for the dynamical propagation of a mode III crack under the action of shear wave will be analysed. One considers the action of constant opposed loading concentrated on boards of the configuration and the other one under the action of a crack face loading that appears behind its moving tip.

3.3.1. ***The crack tip propagation with constant load.*** The out-of-plane displacement $u = u(y_1, y_2, t)$ is obtained by the above 2D finite element analysis for the elastic wave equation under the above conditions, namely the problem is formulated as the following initial-boundary value problem: find a solution $u(y, t)$ which satisfies:

$$\begin{aligned}
&\partial_t^2 u - c^2 \Delta u = 0 \quad \text{in } Q = \cup_{t=0}^{T} \Omega_t, \\
&c^2 \partial_n u = 0 \quad \text{on } \sigma_t, \\
&c^2 \partial_n u = q \quad \text{on } \Gamma_N \times (0, T), \\
&u = 0 \quad \text{on} \quad \Gamma_D \times (0, T), \\
&u(y, t_0) = k(t_0)\, S_N(y_1 - h, y_2, t_0) \quad \text{in } \Omega_{t_0}, \\
&\partial_t u(y, t_0) = 0 \quad \text{in } \Omega_{t_0},
\end{aligned} \tag{3.6}$$

In the first example we deal with the coupled problem (3.6) and (1.1) with a constant load q on $\Gamma_N = \Gamma_{N_1} \cup \Gamma_{N_2} \cup \Gamma_{N_3} \cup \Gamma_{N_4}$.
The left part of the square, see fig. 4 is clamped indicating the Dirichlet boundary of the displacement u, i.e.

$$\Gamma_D = \{(y_1, y_2) : y_1 = -1, -1 \leq y_2 \leq 1\}.$$

and on the remaining boundary Neumann data are specified. We take homogeneous Neumann boundary conditions, $q = 0$, this means no load on:

$$\begin{aligned}
\Gamma_{N_1} &= \{(y_1, y_2) : y_1 = 1, -1 \leq y_2 \leq 1\} \\
\Gamma_{N_2} &= \{(y_1, y_2) : h\,(t) \leqslant y_1 \leqslant 1, y_2 = 0\} = \{(y_1, y_2) \in \sigma_t\}
\end{aligned}$$

and a constant load $q = \pm\, c^2 * 10^{-4}$ on:

$$\Gamma_{N_3} = \{(y_1, y_2) : -1 \leq y_1 \leq 1, y_2 = 1\};$$
$$\Gamma_{N_4} = \{(y_1, y_2) : -1 \leq y_1 \leq 1, y_2 = -1\};$$

see Fig.4, respectively.

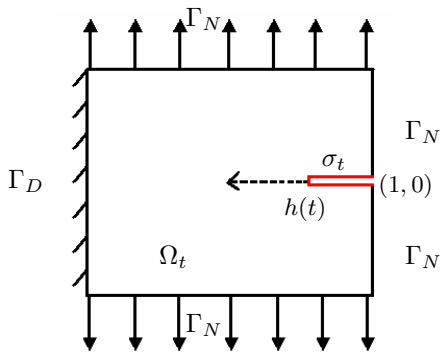

Figure 4: A cracked elastic plate subject to a constant load.

3.3.2. ***Displacement field***. We consider the elastic displacement field $u(y_1, y_2, t)$ along lines parallel to the crack line but in the immediate vicinity of the crack zone, e.g. $y_2 = 0.1$ and $y_2 = -0.1$. It is numerically obtained in the elastic plate, which is assumed to contain one single crack in its interior, i.e. $h_0(t) = 0.9$. A Galerkin method with adaptively generated grid with respect to the growing crack is applied for solving (3.6).

Figure 5 shows the elastic displacement fields $u(y_1, y_2, t)$, for given symmetric y_2 values and for a time t very close to the crack initiation, e.g. $t = 3{*}10^{-5}$ s, produced by the interaction of the crack and the incident wave. It is to be remembered that the pre-crack in the configuration with length $0.1m$ ($h_0 = 0.9m$) is situated at the mid-plane of the square and on the right side (Fig.4). The out-of-plane displacement $u(y, t)$ is obtained by finite element analysis with the PDE2D software program. The displacement field is anti-symmetric with respect to horizontal axis, i.e. u has the property that $u(y_1, -y_2, t) = -u(y_1, y_2, t)$. A finite spike at the time close to the crack initiation is observed, in Fig. 5.
Results for different instants of time $t_1 < t_2 < t_3$... after the crack initiation $t = t_0$ can be also analysed as shown in Figure 6. The results show that even for a point which is relatively close to the crack zone or for times very close to crack initiation time the diffracted stress waves radiate from the crack-tip and propagate into the body. The crack started to grow at some later time. It is to remark that the Figures 5 and 6 are to read from right to left.

3.3.3. ***Dynamical stress intensity factor***. One of the most important parameters in dynamic fracture mechanics is the dynamic stress intensity factor, since it is an important crack-tip characterizing parameter for assessing the propagation of the crack, [11]. It characterizes the stress field in the vicinity of the crack and controls the crack growth. In the present approach $k(t, h, h')$ it is extracted from the displacement field decomposition.
The influence of the waves on the stress intensity factor values at the crack tip is described in the following.
We calculate the leading stress intensity factor $k(t, h, h')$ in (3.6) using formula (3.1):

$$\lim_{R(t)-h_0(t_0)\to 0} \frac{2}{\sqrt{\alpha}} \sqrt{(R(t) - h_0(t_0))} \frac{\partial u}{\partial y_2}|_{\vartheta=0} = k(t_0, h_0, h_0').$$

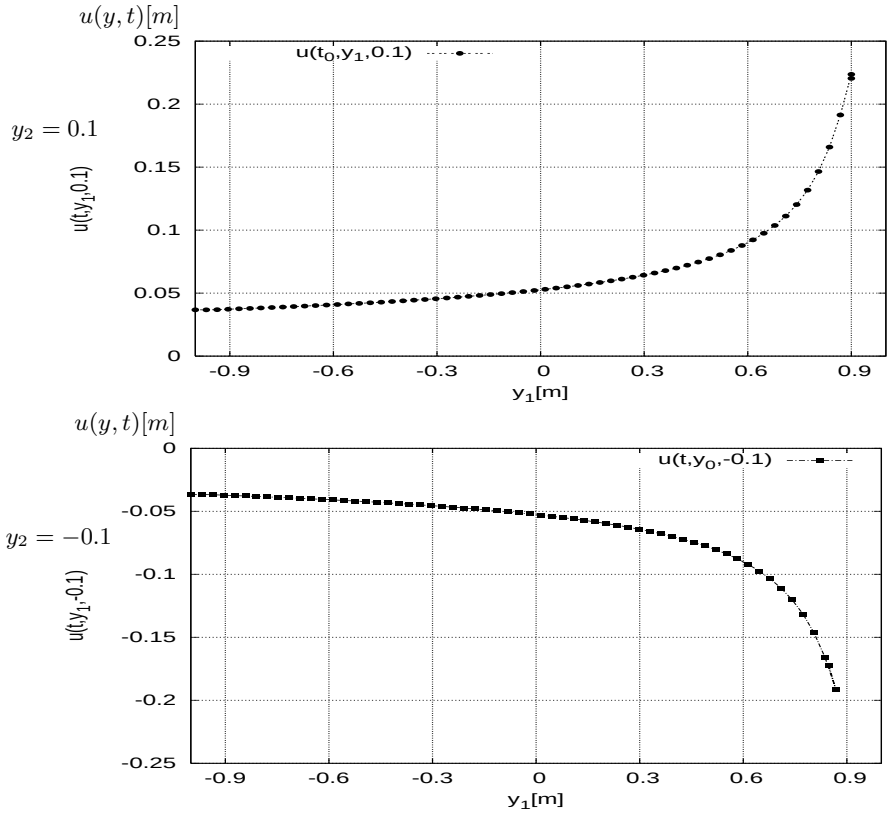

Figure 5: Distribution of the displacement fields $u(y,t)$ along lines parallel to the crack surface for the cracked elastic plate, with constant load ($y_2 = 0.1$, $y_2 = -0.1$, $-1 < y_1 < 1$).

An initial value of $k(t_0, h_0, h_0') = 1$ was assigned with the numerical intent that the initial data for $u(y,t_0)$ in (3.6) and the unknown h' solved by (3.5) be well-defined.
The variation of the estimated dynamic stress intensity factor normalized with respect to their static values versus time is plotted in Figure 7, where an initial crack tip position $h_0(t) = 0.9m$ is supposed.
The stress intensity factor $k(t,h,h')$ from the initial values is:

$$k(t_0, h_0, h_0') = 1.$$

Finally the approximate values of $k(t,h,h')$ were calculated via (3.1) after computing $h(t)$ via (3.5). In Table 1 the approximations of this initial value using increasing number of triangles N in the mesh are shown. Also the relative error is here computed. The plane wave, mathematically defined in (3.6), loads the crack and causes dynamic initiation and propagation of the crack-tip $h(t)$. By solving now the equation of motion (1.1) with the afore extracted dynamic stress intensity factor $k(t,h,h')$, the instantaneous time-dependent crack-tip speed $h'(t)$ can be determined (see iterative procedure). The iterative solution of these two coupled problems provides the solution of the problem of dynamic crack propagation in a 2D-elastic body, under Mode III load.

3.3.4. ***Crack tip speed and crack tip position.*** Figure 8 shows the numerical predictions in which we have used the equation of motion (1.1) to simulate the crack non-uniform velocity $h'(t)$ for the considered pre-crack.

The crack tip speed profile shape for this case in Fig.8 is somewhat similar to that of the second numerical example with time-depending load, Fig.15, but it is smaller in magnitude. The non-uniform velocity motion of the crack tip during which the crack is influenced by incoming

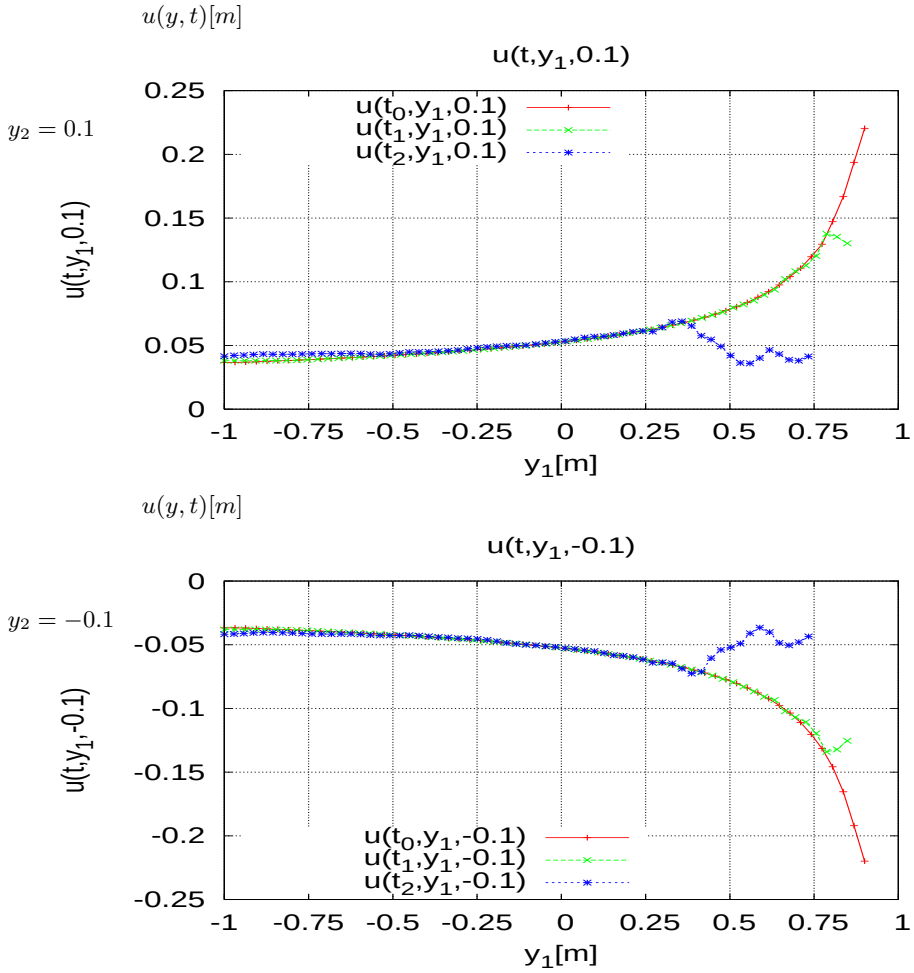

Figure 6: Distribution of the dynamic displacement fields along lines parallel to the crack surface ($y_2 = 0.1$, $y_2 = -0.1$, $-1 < y_1 < 1$) as wave propagates with constant load.

waves, starts from an equilibrium state and changes -more or less -abruptly in comparison to the propagation of crack tip subject to crack face loading.
If the crack grows, the stress intensity factor immediately takes on the value associated with this field. The relation between $k(t, h, h')$ and $h'(t)$ is observed in Figures 7 and 8, when $k(t, h, h') \to 0$ then $h'(t) \to 0$ and when $k^2(t, h, h')$ grows, $h'(t)$ grows also. In Figure 9, the profile of the crack-tip position is plotted.

3.3.5. ***Energetic investigations***. The kinetic energy given in (2.23) is computed here, which is plotted over time in Fig.10. It can be seen that from the beginning of the crack propagation more and more energy is released.

3.3.6. ***Time-dependent crack face loads***. In this section we carry out numeri-
cal simulations of the coupled problem with a pair of opposed concentrated time-dependent forces on the crack surfaces, see Fig. 11. The problem is formulated as the following initial-boundary

$k(t)/k(t_0)$

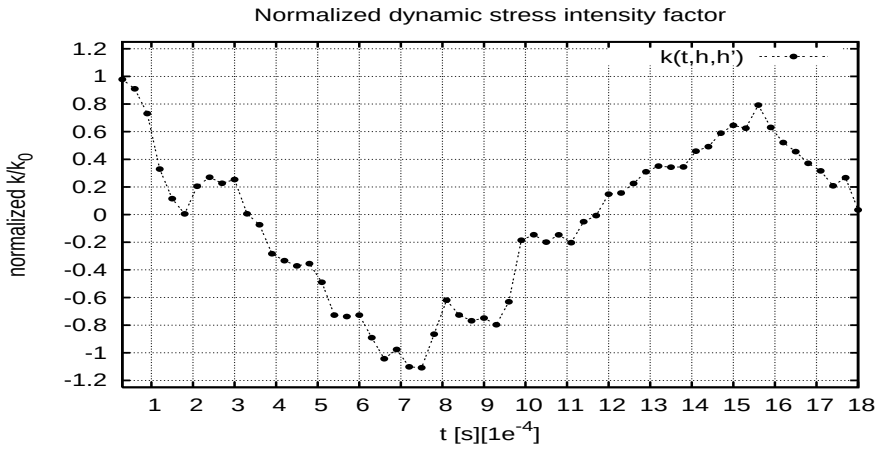

Figure 7: The normalized dynamic stress intensity factor history at the running crack-tip under stress wave loading conditions for initial crack length $0.1m$.

relative error in the approximation of $k(t_0, h_0, h_0')$		
N	computed initial data $k(t_0)$	relative error
40	0.654543409902305	3.4546E-01
96	0.810091530208281	1.8991E-01
192	0.982932043744168	1.7068E-02
500	1.049498245450340	4.9498E-02
1000	0.836843884823183	1.6316E-01
1500	1.031044718215590	3.1045E-02
2500	0.934269479097221	6.5731E-02
3000	1.032540998781370	3.2541E-02
4000	0.993258818271721	6.7412E-03

Table 1: Relative error of initial data for the stress intensity factor

value problem: find a solution $u(y,t)$ which satisfies

$$\begin{aligned}
&\partial_t^2 u - c^2 \Delta u = 0 \quad \text{in } Q = \cup_{t=0}^{T} \Omega_t, \\
&c^2 \partial_n u = c^2\, k(t_0)\, \partial_{y_2} S_N(y_1 - h, y_2, t_0) \quad \text{on } \sigma_t, \\
&c^2 \partial_n u = 0 \quad \text{on } \Gamma_N \times (0,T), \\
&u = 0 \quad \text{on} \quad \Gamma_D \times (0,T), \\
&u(y,t_0) = k(t_0)\, S_N(y_1 - h, y_2, t_0) \quad \text{in } \Omega_{t_0}, \\
&\partial_t u(y,t_0) = 0 \quad \text{in } \Omega_{t_0},
\end{aligned} \tag{3.7}$$

Numerical calculations have been carried out for a cracked square configuration of side-length 2. The configuration contains a pre-crack of length 0.1 m and the crack is assumed to grow straight along the horizontal axis to the left due to the stress distributions on the crack lips.

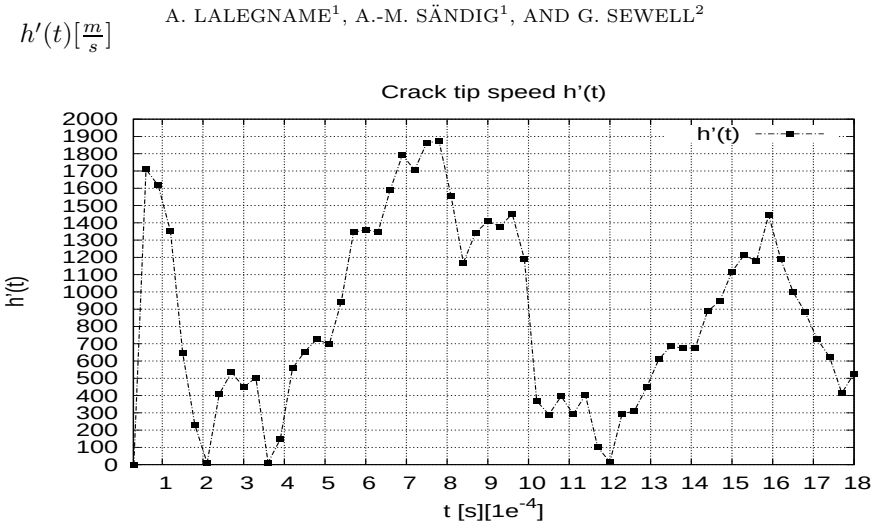

Figure 8: Numerical crack-tip speed for initial crack length $0.1m$.

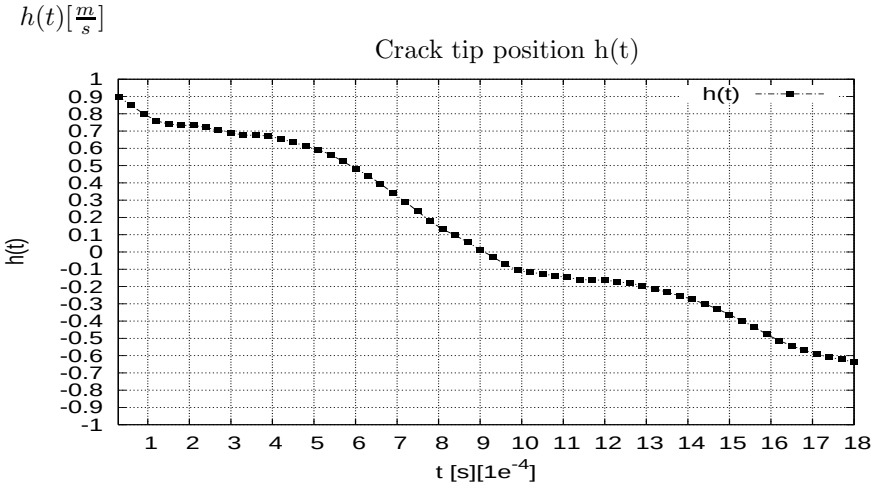

Figure 9: Numerical crack-tip position for initial crack length $0.1m$.

For the displacement field $u(y,t)$, which is a solution of the elastic wave equation in the square R, we impose homogeneous Neumann boundary conditions on $\Gamma_{N_1} \cup \Gamma_{N_2} \cup \Gamma_{N_3}$, (see Fig.11):

$$\Gamma_{N_1} = \{(y_1, y_2) : -1 \leq y_1 \leq 1, y_2 = 1\};$$
$$\Gamma_{N_2} = \{(y_1, y_2) : -1 \leq y_1 \leq 1, y_2 = -1\};$$
$$\Gamma_{N_3} = \{(y_1, y_2) : y_1 = 1, -1 \leq y_2 \leq 1\}$$

and homogeneous Dirichlet boundary condition on:

$$\Gamma_D = \{(y_1, y_2) : -1 \leq y_2 \leq 1, y_1 = -1\}.$$

On

$$\Gamma_{N_4} = \{(y_1, y_2) : h\,(t) \leqslant y_1 \leqslant 1, y_2 = 0\} = \{(y_1, y_2) \in \sigma_t\}$$

a time-dependent load is applied which induces a Mode III-loading on the configuration. The load is thus applied on the newly created crack surface of σ_t.

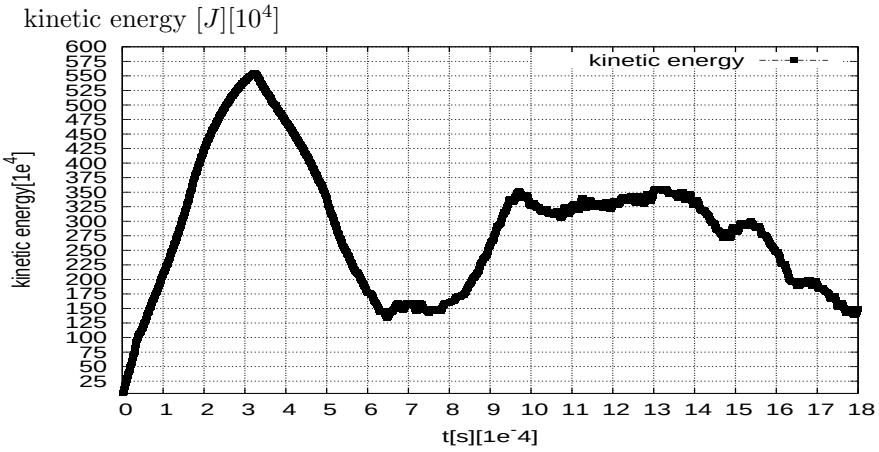

Figure 10: Kinetic energy vs. time for the cracked-specimen.

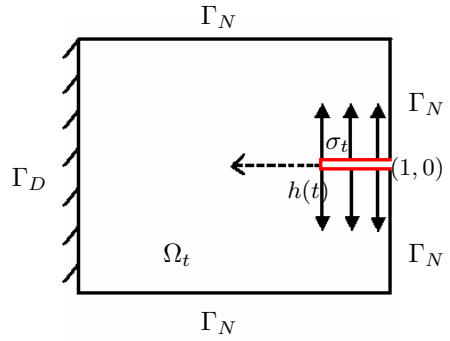

Figure 11: A cracked elastic plate subject to a time-dependent load on the surfaces of the crack.

3.3.7. ***Displacement field.*** For the problem at hand, the full field analytical solution for the elastodynamic field surrounding the crack tip was obtained by formula (1.2). Also, the corresponding dynamic Neumann singular functions in the actual configuration is given by formula (1.3).
The elastic displacement field $u(y_1, y_2, t)$ is considered along lines parallel to the crack line but in the immediate vicinity of the crack zone, e.g. $y_2 = 0.1$ and $y_2 = -0.1$. It is numerically obtained in the elastic plate, which is assumed to contain one single crack in its interior, i.e. $h_0(t) = 0.9m$. A Galerkin method with adaptively generated grid with respect to the growing crack is applied for solving (3.7).

The interaction of the crack and the incident wave is shown in Figure 12 for the elastic displacement field $u(y_1, y_2, t)$, for given symmetric y_2 values and for a time t very close to the crack initiation time, e.g. $t = 3*10^{-5}$ s. It is to be remembered that the pre-crack in the configuration with length $0.1m$ ($h_0 = 0.9m$) is situated at the mid-plane of the square and on the right side, Fig.11. The out-of-plane displacement $u(y, t)$ is obtained by finite element analysis with the PDE2D software program. The displacement field is anti-symmetric with respect to horizontal axis, i.e. u has the property that $u(y_1, -y_2, t) = -u(y_1, y_2, t)$.
In Figure 13 results are shown for different instants of time $t_1 < t_2 < t_3$... after the crack initiation time $t = t_0$.

3.3.8. ***Dynamical stress intensity factor.*** We notice that the dynamical stress intensity factor $k = k(t, h, h')$ plays a key rule in the above problem (3.7), since the coupling of the wave with the motion of the crack is expressed by nonlinear relations between the motion $h(t)$, its velocity $h'(t)$,

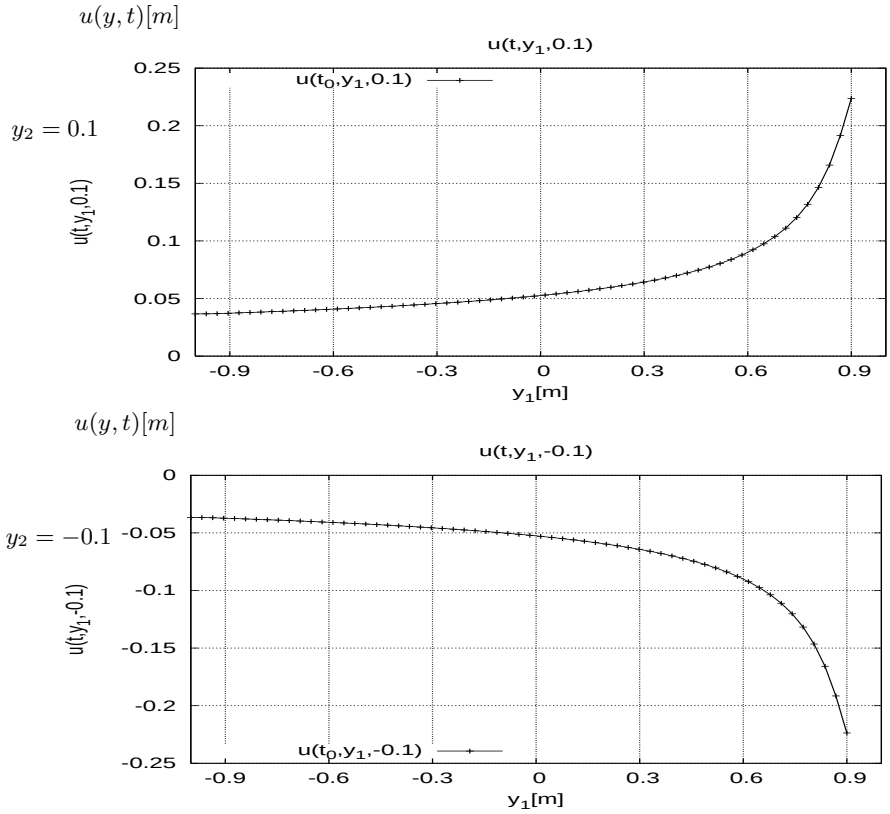

Figure 12: Distribution of the displacement fields $u(y,t)$ along lines parallel to the crack surface for the cracked elastic plate ($y_2 = 0.1$, $y_2 = -0.1$, $-1 < y_1 < 1$).

the dynamic stress intensity factor $k(t) = k(t,h,h')$ and the fracture toughness $\Gamma(h,h')$ given by (3.4). The dynamic stress intensity factor characterizes the stress field in the vicinity of the crack, and controls the crack growth. Here, $k(t,h,h')$ belongs to (3.7) and is extracted by formula (3.1)

Also here an initial value of $k(t_0,h_0,h_0') = 1$ is used, so that the initial data for $u(y,t_0)$ in (3.7) and (3.5) are well-defined.
In Figure 14 the normalized estimated dynamic stress intensity factor versus time is plotted, with an initial crack tip position supposed in $h_0(t) = 0.9m$.

From Fig.(14) it can be determined that the stress intensity factor pattern shown for this particular load is quite similar to that of the previously analysed case, Fig. (7), thus indicating that the stress waves are interacting similary in both cases.

The interaction of the stress wave with the cracked square configuration gives rise to a dynamic stress intensity factor. Once the wave reaches the crack-tip, $k(t,h,h')$ decreaces rapidly to a minimum and it increases thereafter until a peak is reached as t increases further. Subsequent wave interactions lead to an oscillation of $k(t,h,h')$ as Figure 14 reveals. The dynamic of the stress intensity factor depends on many factors, such as the loading rate and other loading conditions, the material characteristics, the geometrical configuration.

The stress intensity factor $k(t,h,h')$ from the initial values is:

$$k(t_0,h_0,h_0') = 1$$

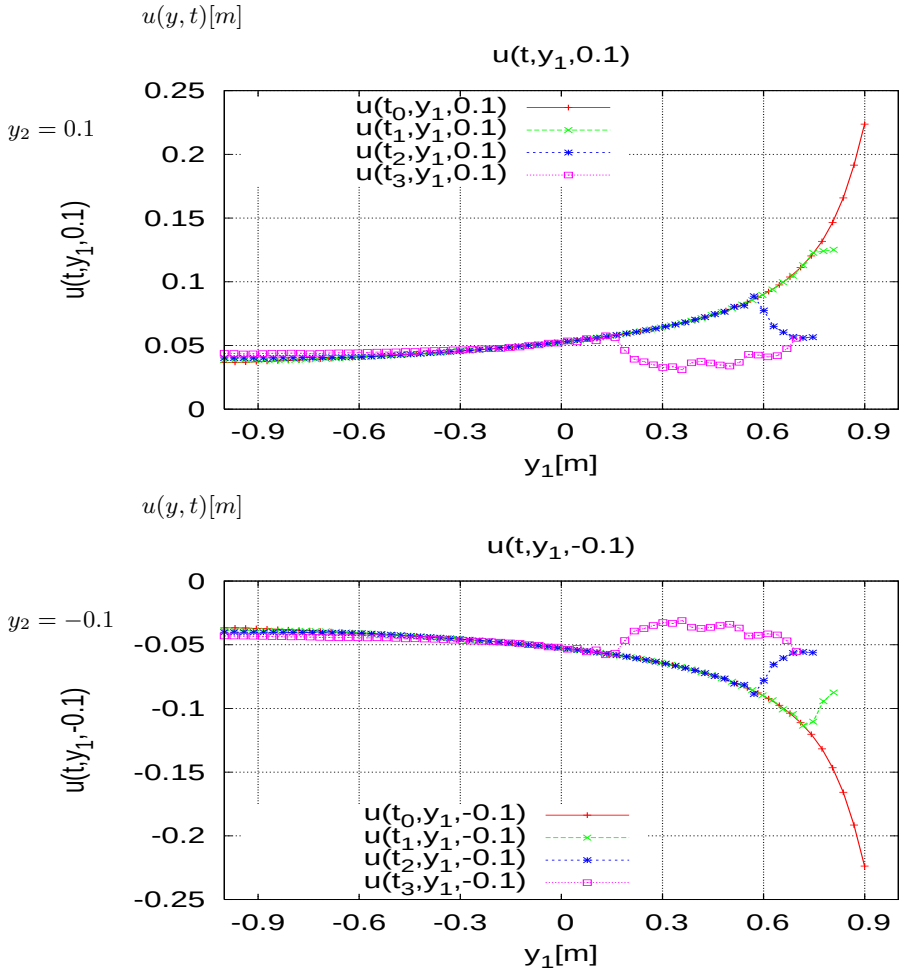

Figure 13: Distribution of the dynamic displacement fields along lines parallel to the crack surface ($y_2 = 0.1$, $y_2 = -0.1$, $-1 < y_1 < 1$) as wave propagates .

and the approximate values were calculated via (3.1). In Table 2 the approximations of this initial value using increasing number of triangles N in the mesh are shown. Also the relative error is here computed.
The plane wave, mathematically defined in (3.7), loads the crack and causes dynamic initiation and propagation of the crack-tip $h(t)$. By solving now the equation of motion (1.1) with the afore extracted dynamic stress intensity factor $k(t, h, h')$, the instantaneous time-dependent crack-tip speed $h'(t)$ can be determined (see iterative procedure). The iterative solution of these two coupled problems provides the solution of the problem of dynamic crack propagation in a 2D-elastic body, under Mode III load.

3.3.9. ***Crack tip speed and crack tip position.*** Figure 15 shows the numerical predictions in which we have used the equation of motion (1.1), to simulate the crack non-uniform velocity $h'(t)$ for the considered pre-crack.

A general belief seems to prevail that crack propagation velocities cannot exceed elastic wave velocities in a material. There are two important reasons for this: first, classical crack propagation theories are very definite in predicting an upper limit for crack velocity which is never greater than some wave velocity (for a review see reference [9]), and secondly, despite an extensive body of crack velocity data, a measurement exceeding the speed of the pertinent wave has not been

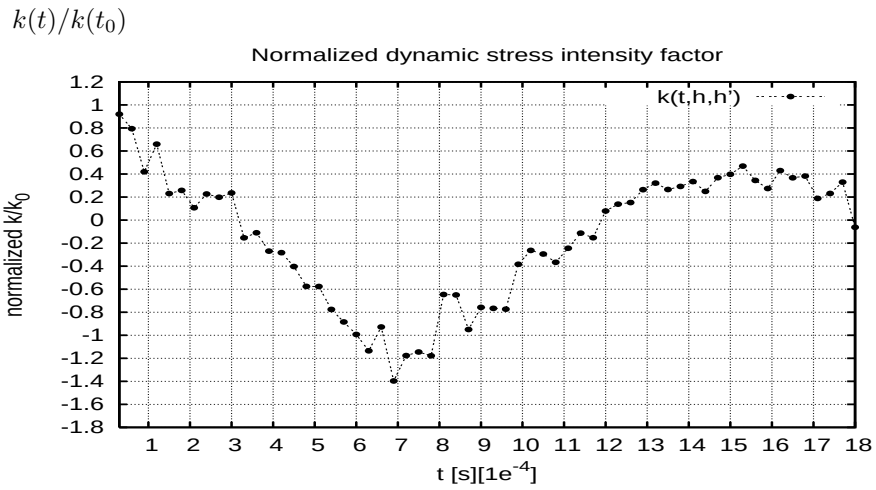

Figure 14: The normalized dynamic stress intensity factor history at the running crack-tip under stress wave loading conditions for initial crack length $0.1m$.

relative error in the approximation of $k(t_0, h_0, h_0')$		
N	computed initial data $k(t_0)$	relative error
40	0.623345345137086	3.7665E-01
96	0.815320427197278	1.8468E-01
192	1.021624515490880	2.1625E-02
500	1.041805932372760	4.1806E-02
1000	0.816402081179707	1.8360E-01
1500	1.044205187069010	4.4205E-02
2500	0.919445110546957	8.0555E-02
3000	1.024602881085090	2.4603E-02
4000	1.011901594303770	1.1902E-02

Table 2: Relative error of initial data for the stress intensity factor

reported.
From an experimental point of view, Ravi-Chandar and Knauss (1984)[27] studied dynamic fracture propagation. Based on their observations, the maximum speed of a Mode-III crack in homogeneous material is about $\approx 0.6 * c$
When the wave hits the crack, the crack begins to grow with non-uniform speed, [30]. At the instant of crack initiation, the crack first jumps from stationary ($h'(t) = 0$) to a velocity about $0.52 * c$, after that the crack-tip speed decreases and increases again and approaches the maximum observed value of $0.63 * c$. We conclude that at least qualitatively this numerical simulation fits with the experimental investigations.
Once the crack-tip speed history $h'(t)$ is known, the time history $h(t)$ of the crack-tip position can be also obtained by integrating the crack-tip speed profile. By applying the equation of motion (1.1), which is coupled with the wave equation (3.7), we have been able to determine the time histories of the non-uniform crack-tip speed and the crack-tip position. In Figure 16, the profile of the crack-tip position is plotted.

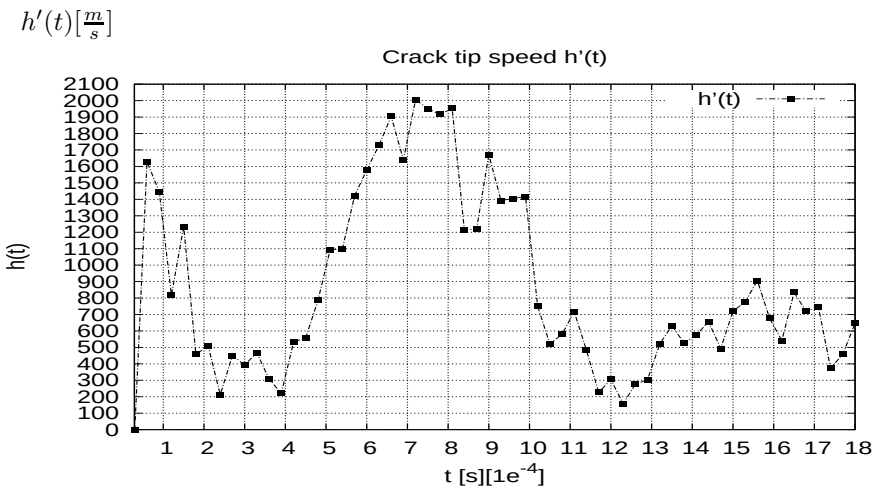

Figure 15: Numerical crack-tip speed for initial crack length $0.1m$.

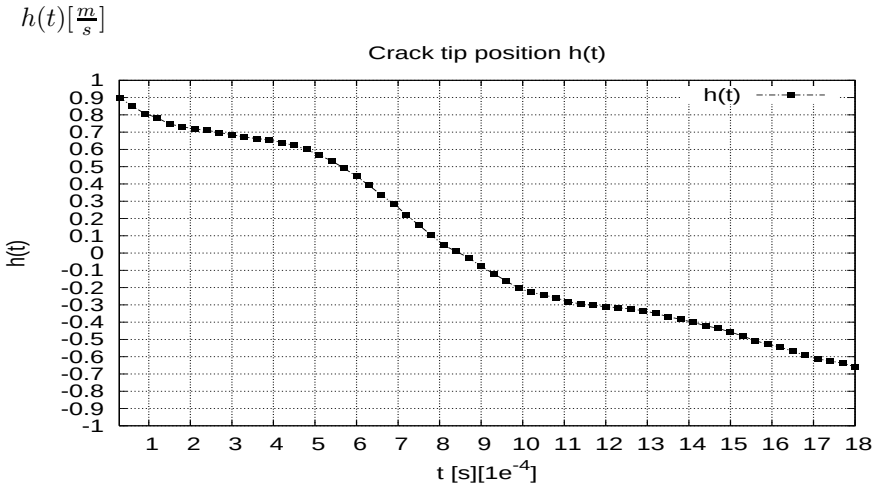

Figure 16: Numerical crack-tip position for initial crack length $0.1m$.

3.3.10. ***Energetic investigations.*** We carry out an energetic investigation for the elastic medium with a single crack. It was found above that in formulating the theory of crack propagation the problem of energy dissipation must be examined.

The analysis in this problem for a configuration containing a moving crack can be defined by local and global approaches. The local approach considers the singular elastic displacement field in the vicinity of the crack-tip, see (1.2). The singularity associated with this field is characterised by a parameter called the stress intensity factor $k(t, h, h')$, see (3.1). On the other hand, the global approach is concerned with the total energy balance in the body and describes the crack growth in terms of the energy release rate G, and the fact that $\dot{D}(t) = G(h, h')h'(t) = \Gamma(h, h')h'(t)$, see (2.20).
The problem of the energy dissipation in the process of crack propagation has been completely settled by the corresponding energy definitions (2.21, 2.22 and 2.23), as well as the energy balance law (2.20).
The kinetic energy of the system is evaluated by direct computation of the integral (2.23), using the solution of displacement u of (3.7). Figure 17 shows that the kinetic energy rises to a maximum

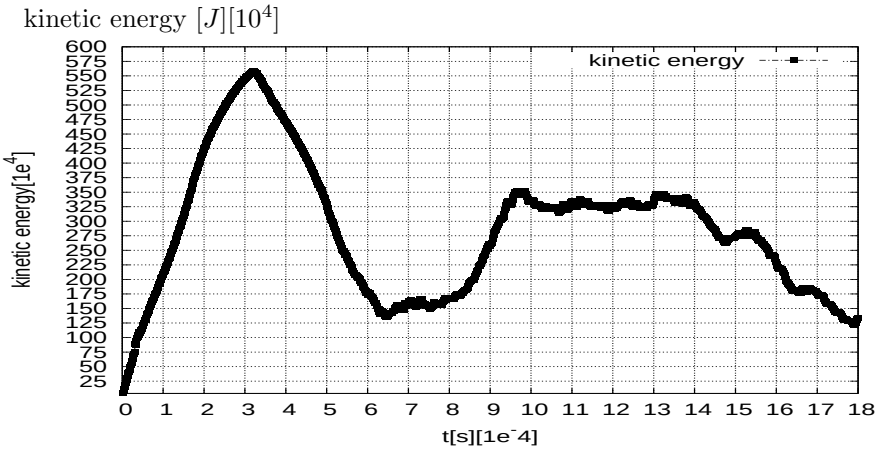

Figure 17: Kinetic energy vs. time for the cracked-specimen.

at about the crack length $l = 0.33$, i.e. the crack tip position point $h(t) = 0.67m$ and crack tip speed $h'(t) = 467\frac{m}{s}$. The subsequent decrease seems to indicate the reflexion of waves from the boundaries.
The figure 18 shows a surface plot for the cracked region, whose boundary was defined by the problem (3.7).

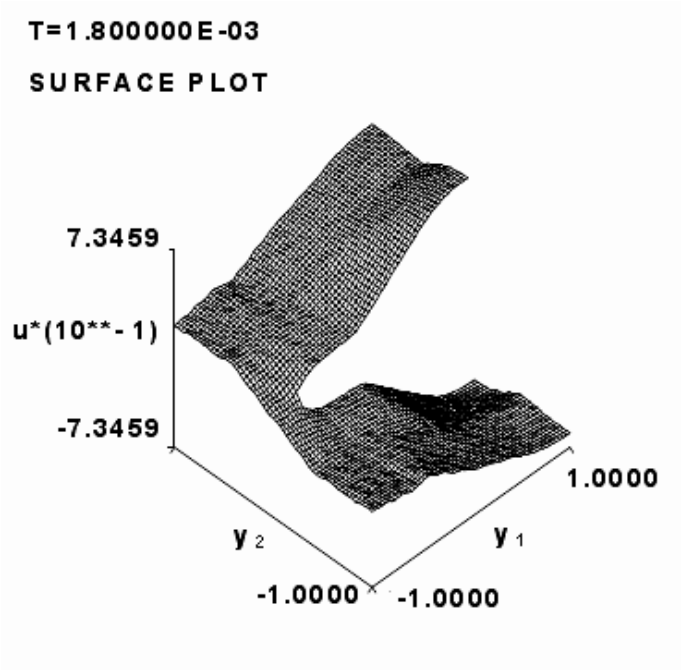

Figure 18: Surface Plot.

3.4. **Conclusion.** A rigorous mathematical derivation of the crack tip motion under the influence of a wave is given in Section 2, which represents a completion of the paper [22].
Numerical approximation methods for this coupled problem are developed in Section 3. We focus on the development of stable methods, as Crank Nicholson, Galerkin methods [15], [34]. In this

context, stable means that no overshoots or undershoots occur. In section 3 an iterative procedure is derived for the coupled problem. Here the initial value of the dynamical stress intensity factor plays the role of a stabilisation term, where the $\Gamma(h, h')$ coefficient is used as a stabilisation parameter and $\Gamma(h, h') = \beta * \dfrac{1-\alpha}{\alpha}$.

In numerical simulations of dynamic crack propagation, one must treat a moving-singularity. Since the moving singularity induces various errors in numerical models, it is critical to develop accurate solution procedures for the advancement of fracture mechanics. In this work, it is assumed that the crack always propagates along a straight line and it does so under the influence of a wave.

So far, to the authors' knowledge, no such simulations for crack propagation have been done.

The set of coupled equations (3.6), (3.7) and (1.1) is solved by the program PDE2D, a commercially-available finite element code (www.pde2d.com). The grid of the calculation must be particularly dense near the crack tip. A final triangulation of 4000 quadratic triangles is used. The analysis shows that -as expected- the coupled problem for the crack propagation with the interaction of a wave reproduces the characteristics of material behaviours, such as the stress intensity factor, the crack tip speed and the crack tip position.

The influence of the geometry and of the length of the pre-existenting crack on the configuration could also be considered, but were not in this study, for more details see [31].

3.4.1. ***Open problems***. The equation of motion of the crack tip under the influence of a wave was simulated here for given initial data, loading and other parameters. The simulation results and data can be used in the future in order to compute the crack tip propagation behaviour in other situations, which may be important for industrial applications. Although no experimental justification for the here used formula for $\Gamma(h, h')$, or any other, the software developed in this paper can be easily adapted to experimentally justified fracture toughness formulas, when such are available.

References

[1] Atluri,S.N. & Nishioka, T. Numerical studies in dynamic fracture mechanics, Dynamic Fracture, ed. M.L. Williams & W.G. Knauss, Martinus Nijhoff Publishers, 1985, pp. 119-135.

[2] Buehler, M.J., Gao H., Huang Y. Atomistic and continuum studies of a suddenly stopping supersonic crack Computational Materials Science 28, 2003, pp. 385-408.

[3] Brenner, S.C. and Scott L.R. The mathematical theory of finite element methods. Springer Verlag, 1994.

[4] Broberg, K.B. Cracks and Fracture, San Diego, Calif. [u.a.]:Academic Press, 1999.

[5] Ciarlet, P. G. The Finite Element Method for Elliptic Problems. North-Holland Publishing Company, 1976.

[6] Charoenphan, S. Computer methods for modeling the progressive damage of composite material plates and tubes. PHD Thesis at University of Wisconsin-Madison, 2002.

[7] Dauge, M. Elliptic Boundary Value Problems on Corner Domains, Lecture Notes in Mathematics 1341, Springer-Verlag, Berlin-Heidelberg, 1988 MR 91a:35078.

[8] Destuynder, P., Jaoua, M. Sur une interprétation mathématique de l'intégrale de Rice en théorie de la rupture fragile, Math.Methods Appl.Sci.3, 1981, pp. 70-87.

[9] Erdogan, F. Crack-Propagation Theories, Chapter 5 in Fracture Vol. II, Liebowitz ed., Academic Press, New York and London, 1968.

[10] Freund, L.B. Crack propagation in an elastic solid subjected to general loading III. Stress wave loading, Journal of the Mechanics and Physics of Solids 21, 1973, pp.47-61.

[11] Freund, L.B. and Clifton, R.J. On the uniqueness of plate elastodynamic solutions for running cracks, Journal of Elasticity, 4(4), 1974, pp.293-299.

[12] Freund, L.B. Dynamic Fracture Mechanics, Cambridge University Press, New York, 1990.

[13] Grisvard, P. Elliptic Problems in Nonsmooth Domains, Pitman, Boston, 1985, MR 86m:35044.

[14] Gross, D. Bruchmechanik, Springer-Verlag, Berlin, 1996.

[15] Großmann, C., Roos, H.-G., Numerische Behandlung partieller Differentialgleichungen. B.G. Teubner Verlag, 2005

[16] Kerkhof, F. Habilitationsschrift, Karlsruhe, 1965.

[17] Kobayashi, A.S. and Mall, S. Dynamic fracture toughness of Homalite 100, Experimental Mechanics, 18, 1978, pp.11-18.

[18] Kondrat'ev, V. A. Boundary value problems for elliptic equations in domains with conical or angular points, Trans. Moscow Math. Soc. 16, 1967, pp. 227-313.

[19] Koslov, V.A., Maz'ya, V.G., Rossmann, J. Elliptic Boundary Value Problems in Domains with Point Singularities, Amer. Math. Soc., Providence, RI, 1997.

[20] Maz'ya, V.G., Plamenevskii, B.A. On the coefficients in the asymptotics of the solutions of an elliptic boundary value problem in domains with conical points, J. Soviet Math.9, 1978, pp. 750-764.

[21] Nazarov, S.A., Plamenesvkii, B.A., Elliptic Problems in Domians with Piecewise Smooth Boundaries, Expositions in Mathematics, vol.13, de Gruyter, Berlin, New York, 1994, MR 95h:35001.

[22] Nicaise, S., Sändig, A.-M. Dynamical crack propagation in a 2D elastic body. The out-of plane state. J. Math.Anal. Appl. 329, 2007, pp. 1-30.

[23] Nishioka, T.& Atluri, S.N.. Computational methods in dynamic fracture, Computational Methods in the Mechanics of Fracture, Chapter 10, ed.S.N. Atluri, Elsevier Science Publishers, 1986, pp.335-383.

[24] Ohyoshi,T. Effect of Orthotropy on singular stresses produced near a crack tip by incident SH-waves. ZAMM 53, 1973, pp. 409-411.

[25] PDE2D, Sewell, G. University of Texas, El Paso. www.pde2d.com.

[26] Ravi-Chandar, K. and Knauss, W.G. Dynamic crack-tip stresses under stress wave loading - A comparison of theroy and experiment, International Journal of Fracture, 20, 1982, pp.209-222.

[27] Ravi-Chandar, K. and Knauss, W.G. An experimental investigation into the mechanics of dynamic fracture: I. Crack initiation and arrest, International Journal of Fracture, 25, 1984, pp.247-262.

[28] Ravichandran, G. and Clifton, R.J. Dynamic fracture undr plane wave loading, International Journal of Fracture, 40, 1989, pp-157-201.

[29] Rosakis, A. J., Duffy, J. and Freund, L.B. The determination od dynamic fracture toughness of AISI 4340 steel by the shadow spot method, Journal of Mechanics and Physics of Solids, 32, 1984, pp.443-460.

[30] Rosakis, A.J., Liu, C. and Freund, L.B. A note on the asymptotic stress field of a non-uniformly propagating dynamic crack, International Journal of Fracture, 50, 1991, R39-R45.

[31] Sändig, A.-M., Nicaise, S., Lalegname, A. Dynamic crack propagation in a 2D elastic body. The out-of plane case. ICIAM 07. ETH Zürich, 2007.

[32] Schwab.C. P-and hp-Finite Element Methods. Oxford University Press, 1998.

[33] Seelig, Th.: Zur Simulation der dynamischen Rißausbreitung mit einer Zeitbereichs-Randelementmethode. Ph.D. Thesis, TH Darmstadt, Germany, 1997.

[34] Sewell, G. The Numerical Solution of Ordinary and Partial Differential Equations Second Edition. John Wiley & Sons Inc. June 2005.

[35] Suresh S. Fatigue of Materials Cambridge University Press 1998, 2nd edition.

[36] www.sv.vt.edu/classes/MSE2094_NoteBook/97ClassProj/exper/gordon/www/fractough.html

[37] Williams, T. e al. GnuPlot, version 4.0. Technical report, Pixar Corporation, http://www.gnuplot.info/ 2004.

[38] Zehnder, A.T. and Rosakis, A.J. Dynamic fracture initiation and propagation in 4340 steel under impact loading, International Journal of Fracture, 43 (4), 1990, pp.271-285.
[39] Zhang, Ch. and Gross, D. Interaccion of Antiplane Cracks with Elastic waves in transversely isotropic materials. Acta Mechanica 101, 1993, pp. 231-247.
[40] Zhang, Ch. On wave Propagation in Cracked Solids. Habilitationsschrift, TH Darmstadt, Germany, 1993.

Erschienene Preprints ab Nummer 2008/001

Komplette Liste: `http://preprints.ians.uni-stuttgart.de`

2008/001 *Perfahl, H., Sändig, A.-M.*: A Continuum-Mechanical Approach to Avascular Solid Tumor Growth

2008/002 *Giesselmann, J.*: A convergence result for finite volume schemes on 2-dimensional Riemannian manifolds

2008/003 *Rohde, C., Surulescu, C.*: Mathematische Modellierung und Analyse von biologischen Prozessen

2008/004 *Lalegname, A., Sändig, A.-M., Sewell, G.*: Analytical and numerical treatment of a dynamic crack model